REFLECTIVE RESPONSE AND VELOCITY DISCRIMINATION IN THE CENTRAL PART OF THE GULF OF SUEZ, EGYPT

Mounir A. Ismail

Geophysics Department, Faculty of Science
Ain Shams University
Cairo, Egypt

الخلاصـة :

تَصِفُ هذه المقالة تأثير شكل الحوض بخليج السويس البحري على تغير السماكة والأنعكاسات (معدل الأنعكاس والمرور)، وتعتبر كقاعدة لمعرفة تأثير الصخور غير المتجانسة على السرعات (البينية والمتوسطة) لبعض التتابعات الأستراتيجرافية في الجزء الأوسط بخليج السويس؛ خصوصاً عند الجزء الجنوبي من حقل بترول بلاعيم ووجدنا أن قيم السرعات العالية يحتمل أن تكون ناتجة عن وجود كتل صخرية غير مفككة (المتبخرات) وقيم السرعات المنخفضة ناتجة من الفتات الصخرى (الطين).

قمنا برسم خرائط تَساوي السماكة والانعكاسيات والسرعات لأربعة تكوينات (زيت – جنوب غارب – بلاعيم – كريم) والتي بدورها تعكس سلوك كلٌ من ظروف الترسيب وتكتونية المنطقة خلفاً للترسيب.

كما وجدنا أن قيم معاملات الانعكاس عادةً موجبة عند أسطح كلٌ من تكويني زيت وجنوب غارب عدا بئر GS 278-1 حيث إنَّ السرعة تزيد للأسفل وفي اتجاة الشمال الشرقي والجنوب الغربي. وعلى النحو الآخر؛ وجد أن القيم السالبة من معاملات الانعكاس تزيد عند أسطح كلٌ من تكويني بلاعيم وكريم (بمعنى آخر وُجد أن السرعة تقل للأسفل.) وهذه المنطقة تقسم الى ستة أحواض ترسيب تأخذ أتجاة الشمال الغربي وإنَّ حيود السرعات يظهر محكماً بتراكيب وتتأثر الموجات الصوتية أثناء سريانها في الصخور الملحية والشعاب المرجانية والقواطع النارية والطبقات المشوهة.

وتحديد مصادر الحيود يسمح بالتنبؤ بأماكن التشوهات في العاكسات المعرفة، وفي بعض الحالات إذا كانت معلومات السرعة كاملة وكافية فمن الممكن إنشاء القطاع السيزمي الصحيح. ويُعَدُ التعامل مع تصحيح السرعات في خليج السويس المفتاح لإعادة معالجة البيانات السيزمية في المنطقة ذوات التركيب المعقدة. وسرعات اللصق (Stacking) عند أفضل تنبؤ بها وجد أنها لا تساوي السرعات المقاسة في البئر وتكون عادة غير مناسبة، وهذا يدفعنا لتصحيح السرعة والمكان الصحيح لالتقاط الموجة المختارة.

لقد رُسمت هذه الخرائط لإمكانية تحديد المعاملات الصوتية لظروف البيئات المختلفة. وقد لوحظ أن خطوات معالجة البيانات السيزمية في الجزء الأوسط من خليج السويس تختلف تماماً عن المناطق الشاطئية. ولوحظ أيضاً أن صخور الميوسين الملحية قد تسببت ليس فقط في تشوهات تركيبية في قطاعات ما بعد الملح، ولكن أيضاً ظهور تشوهات شديدة في الانعكاسات الموجودة فيما قبل الصخور الملحية، وبمقارنة هذه الانعكاسات على القطاعات الملصقة والمهجرة خلال الصخور الملحية اللدنة. نستنتج أن هجرة الزمن غير ملائمة ولكن المعالجة بهجرة العمق هي الصحيحة.

ABSTRACT

This paper describes the effect of basin configuration on the thickness variations and reflectivities (reflection and transmission coefficients), as well as the role of lithologic heterogeneity on the velocities (interval and average) of some stratigraphic sequences in the central part of the Gulf of Suez, principally at the southern part of Belayim Oil Field. The high velocity values may be attributed to the occurrence of massive non clastics (evaporites) and the low velocity ones due to loose clastics (shale). Isopach, reflectivity and velocity maps for four formations (Zeit, South Gharib, Belayim, and Kareem) are constructed, which reflect the behavior of depositional conditions, and the tectonism standing behind the sedimentation.

The reflection coefficient values are generally positive at the tops of Zeit and South Gharib Formations, except at GS 278-1 well, that is the velocity increases downwardly and in the NE–SW direction. On the other hand, the negative values of the reflection coefficient increase at the tops of Belayim and Kareem Formations, *i.e.*, the velocity decreases downwardly. This area is subdivided into six depositional basins trending in the NW-direction. The velocity anomalies appeared to be structurally controlled and are caused by the sound waves going through the salts, reefs, igneous dikes, and distorted beds. It is possible to identify the sources of these anomalies and allow to predict the distortion of the recognized reflectors. In some cases, the velocity data are complete enough to establish a corrected section.

The velocity discrimination in the Gulf of Suez is dealt with; it is considered the key to the seismic re-processing in this complex structural area. The stacking velocities at their best prediction cannot be expected to be equal to the check-shot velocities, unless proper attention is paid to the velocity corrections and to the exact position of the wave pulse selected for picking. All these maps are constructed in order to deduce the acoustic parameters of the different environmental conditions. The processing steps in the central part are completely different from the coastal zones. The Miocene salt causes not only structural deformation in the post-salt sections, but also severe time distortion of the pre-salt reflections. Comparison of the event on stacked and migrated sections through the salt diapir made it obvious that the time migration was inadequate and a depth migration process was required.

REFLECTIVE RESPONSE AND VELOCITY DISCRIMINATION IN THE CENTRAL PART OF THE GULF OF SUEZ, EGYPT

INTRODUCTION

The study area is located at the South Belayim oil field, in the central part of the Gulf of Suez (Figure 1). A large number of exploratory wells were drilled in the Gulf of Suez region. Well data are used for evaluating the subsurface lithology, rock velocity, and rock density. The litho-stratigraphic data are obtained from the composite well logs. A velocity survey was carried out in the South Belayim area to obtain a clear picture about the reflectivity and transmissivity functions for the seismic energy and to relate between the lithologic contents and the behavior of seismic energy. Velocity analyses (average and interval) at different formations were also carried out in order to deduce the acoustic parameters of the different environmental conditions.

GEOLOGIC SETTING

Barakat [1] differentiated the stratigraphy of the Gulf of Suez into three distinct sequences: (1) the Pre-Miocene sediments, that range in age from Devonian to Eocene. They are considered as good reservoir rocks; (2) the Miocene rocks; that are important as source rocks in the Gulf of Suez as a whole; and (3) the Post-Miocene section; that is relatively thin with no importance either as source rocks, or reservoir rocks, or cap rocks for hydrocarbons (Figure 2) [2]. Most of the oil reserves occurred in eight major fields located in the more extensively drilled (central and southern) parts of the Gulf of Suez region with varying productivity as: (1) three fields are producing from the Lower Miocene sandstones; (2) two fields are producing from both the Lower Miocene and Cretaceous Nubia Sandstones; and (3) three fields are producing from the Middle Miocene limestone.

Ismail [3] concluded that there are two major right lateral strike-slip faults trending ENE–WSW and extending from the eastern side of the Sinai plate to the central part of the Gulf of Suez and restricted between them several micro-structures of faults and folds. The faults are oriented in the NW–SE and NNW–SSE directions, while the folds are trending in the N–S direction.

The stratigraphic sequence in the Gulf of Suez province is studied, starting from the basement complex and ending with the Post-Miocene (Figure 2) [2]. The units of Lower Rudeis were detected in all wells, where they are preserved from the intra-Rudeis erosion.

Kareem Formation overlies the Rudeis Formation and is mainly composed of shale, limestone and interrupted by some sand units. It was deposited in a relatively deep marine environment with minor episodes of basin closing. This formation is oil-bearing, like in Morgan and July Oil-Fields. The maximum thickness is 1580 ft in SB 284-1 well. Middle–Upper Miocene (Ras Malaab Group) is one of the famous evaporitic rocks in the North African basins and initially related to the depositional environments in the Red Sea region [4]. Successive cycles of salt and anhydrite rocks can be differentiated on the density and electric logs. In general, the Middle Miocene rocks are considered the cap rocks for the different oil reservoirs underlying them.

Belayim Formation is classified into four members: Baba (anhydrite and shale), Sidri (shale and sand lenses), Feiran (anhydrite and shale), and Hammam Faraun (clastic and carbonate facies, considered the thickest clastic section within the Middle Miocene). The maximum thickness is 1306 ft in 334-3 well.

South Gharib Formation overlies the Belayim Formation and is composed of anhydrite and salt with minor thin shale beds. The maximum thickness is 3300 ft in Alef-1 well. It is thicker at the central parts of the Miocene basins and thinner at the margins, as shown in the area under investigation.

Zeit Formation overlies the South Gharib Formation and consists of shale and evaporites. There is a general thinning of the formation northwards, where it is absent in the extreme northern part of the Gulf. These Miocene evaporites are believed to have originated on the coastal sabkhas (supratidal flats), where no biological organisms could survive the supersaline environment.

AVAILABLE DATA

Among the few wells that penetrated the whole Miocene section, only two had tested the Pre-Miocene. Most of the wells are bottomed in the Kareem Formation, which explain the shortage of data relevant to this formation and those beneath it.

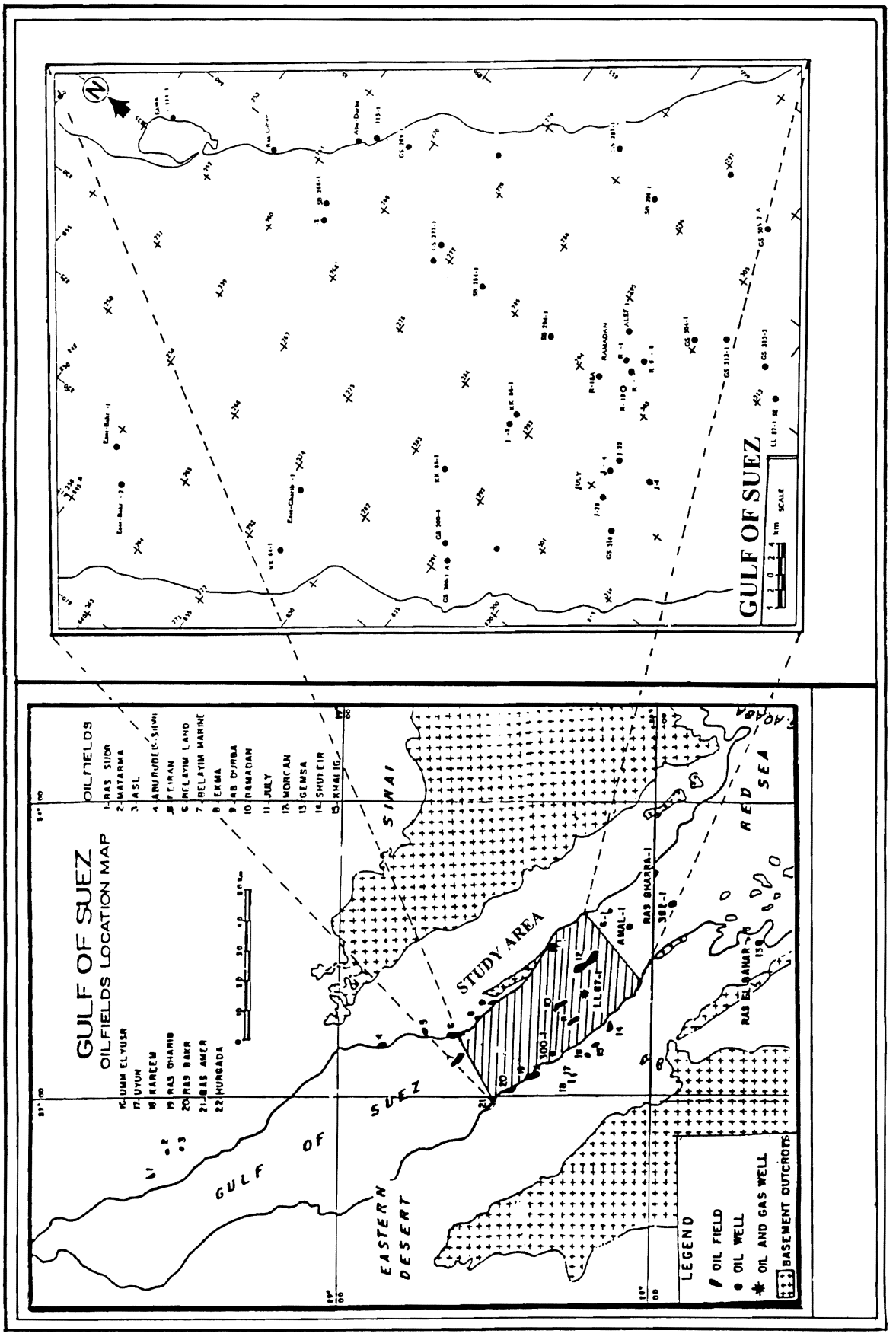

Figure 1. Location Map for South Belayim Area, Gulf of Suez.

Sonic logs and continuous velocity logs (CVL) for most of the studied wells represent the basic source of velocities, while the root mean square velocities are selected for certain shot points across the stacked seismic sections. Moreover, the composite logs of the studied wells are available to detect their litho-stratigraphic sequence and the depths of their formational tops.

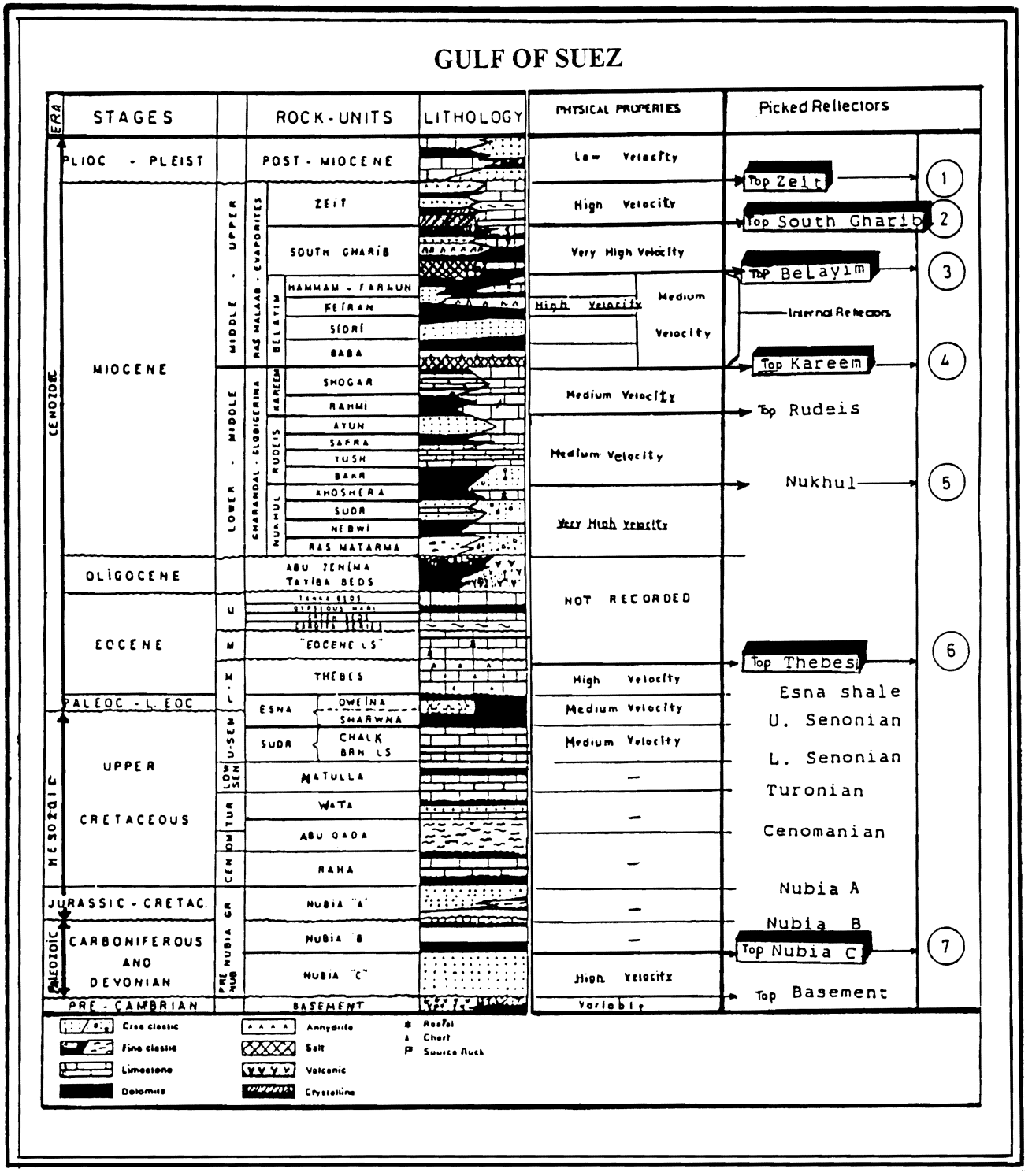

Figure 2. Generalized Litho-Stratigraphy (after Schlumberger, 1984) and Main Seismic Reflectors of the Gulf of Suez (Ismail, 1995a) [3].

ISOPACH RESPONSE

By the end of Rudeis till the Zeit Formation, a considerable abrupt change has occurred. The Post-Zeit sediments were deposited after a major hiatus under continental and paralic environments. The isopach response is examined to establish the main directions of thinning and thickening of the studied formations, the degree of gradation, the shape and extension of the sedimentary basins and their relations to the main tectonism.

The isopach maps are drawn for the Zeit, South Gharib, Belayim, and Kareem Formations. The isopach map of Zeit Formation (Figure 3*a*) shows that, the maximum thickness 4479 ft is located in the central part of the Gulf at J-6 well, while the minimum 76 ft is found towards the coastal lines at Sh.M.1 well. This reflects the fact that the rate of energy loss is increased in the central part, but decreased towards the shore line and accordingly the processing steps in the central part are completely different from those in the coastal zones.

The isopach map of South Gharib Formation (Figure 3*b*) exhibits a variable thickness between 1611 ft and 2990 ft. The isopach map of Belayim Formation (Figure 3*c*) shows its absence in several wells. Its thickness ranges from 100 ft (at E. Baker-1 well) to 1820 ft (at Shukeir M-1 well). The identical thickness variation of Kareem Formation (Figure 3*d*) reflects continuous sedimentation as Belayim Formation. The thickness ranges from 1250 ft (at WM-1 well) to 250 ft (at Shukeir M-2 well). Ismail [3] found that the structural patterns are formed by compressional and/or tangential forces recorded in the NE direction and can be attributed to the rotation of the Sinai plate.

REFLECTIVITY FUNCTION

The subsurface geologic section can be approximated by a series of layers having a specific acoustic impedance (velocity × density), which can also be represented by a series of reflection coefficients at the boundaries. Sonic and density logs can be used to compute the reflectivity series, which can then be convolved with a suitable wavelet like Ricker wavelet.

The acoustic impedance of a rock unit, Z, is defined as:

$$Z = \rho V \tag{1}$$

where: ρ is the bulk density and V is the P-wave velocity. The amount of reflected energy at the interface of two beds depends on the relative impedances of these two beds. For normal incidence, the reflection coefficient was first published in [5]. It involves only two physical parameters; density and velocity, and given by the relation:

$$R = \sqrt{E_r/E_i} = A_r/A_i = (\rho_2 V_2 - \rho_1 V_1)/(\rho_2 V_2 + \rho_1 V_1) \tag{2}$$

where: E_r and E_i are the reflected and the incident energies, respectively, and E_r and E_i are the reflected and the incident wave amplitudes, respectively. The reflection coefficient (R) is defined in terms of acoustic impedances (Z) as:

$$R_{n-1,n} = (Z_n - Z_{n-1})/(Z_n + Z_{n-1}) \tag{3}$$

where: Z_n and Z_{n-1} are the acoustic impedances of the layers n and $n-1$. The reflection coefficient is the ratio of the change in acoustic impedance to twice the average acoustic impedance. If Z_n is greater than Z_{n-1}, then the reflection coefficient would be positive; while if it is inverse, then the reflection coefficient would be negative. The thickness of the reflecting horizon should be considered in comparison with the wavelength of the propagating seismic signal. Theoretically, the minimum thickness of a bed which can probably be seen by the seismic wave is approximately $\cong \lambda/12$ (one-twelfth the wavelength).

Figure 4*a* shows the reflection coefficient map at the top of Zeit Formation. The maximum and minimum values are +0.321 and +0.0875 at Alef-1 and East-Baker M-1 wells, respectively. The reflection coefficient map at the top of South Gharib Formation (Figure 4*b*) exhibits maximum and minimum values of +0.21 and +0.0234 at GS 313-3 and SB 268-1 wells, respectively. All the reflection coefficient values are positive, except at GS 278-1 well that is −0.0652. For both formations, the velocity increases downwardly and areally in the NW direction. Figure 4*c* shows the reflection coefficient map at the top of Belayim Formation, in which the positive values are concentrated at the central part of the gulf. This is due to the change of lithology in the horizontal and vertical directions toward the top of the formation. The reflection coefficient map at the top of Kareem Formation (Figure 4*d*) reflects three positive values only at WM-1, GS 300-4 and E-Baker M-1 wells and negative values at the other wells, with a range between −0.2214 at J-3 well and −0.048 at GS 300-1 well.

TRANSMISSION COEFFICIENT

The transmission coefficient is the ratio of the amplitude of the transmitted wave to that of the incident wave. The two-way transmission coefficient from the first interface is calculated for normal incidence as follows:

$$T_{12} = \left(1 - R_{12}^2\right) = \left(4\rho_1 V_1 \rho_2 V_2\right) / \left(\rho_2 V_2 + \rho_1 V_1\right)^2 \tag{4}$$

where: R_{12} is the amplitude of reflection from the first interface in [6] and the amplitude of reflection from the second interface is $R_{23}\left(1 - R_{12}^2\right)$, while the amplitude of reflection from the third interface is $R_{34}\left(1 - R_{12}^2\right)\left(1 - R_{23}^2\right)$. The ratio of the energy densities is the square of the transmission coefficient in [6]. The transmission and reflection coefficients are inversely proportional.

The transmission coefficient map at the top of Zeit Formation (Figure 5*a*) exhibits a very high rate of energy loss in some locations, where it attains a value of 0.957 at GS 269-1 well and 0.959 at KK 85-1 well. For South Gharib Formation (Figure 5*b*), it attains values of 0.976 and 0.956 at GS 277-1 and GS 313-3 wells, respectively. Figure (5*c*) shows the transmission coefficient map at the top of Belayim Formation, in which the energy loss has its maximum value (0.8867) at GS 278-1 well. The area reveals values ranged between 0.9784 at J-6 well and 0.9993 at GS 300-1 well. The transmission coefficient map at the top of Kareem Formation (Figure 5*d*) shows that a maximum energy loss is located at the central part of 0.9419 at GS 269-1 well and 0.958 at KK 85-1 well, and a decrease elsewhere.

O'Doherty and Anstey [7] discussed the two-way transmission loss through a number of interfaces, for a range of reflection coefficients 0.2, 0.1, and 0.05 (Figure 6: from [7]). A selected example is displayed on the relation between the reflection coefficient at SB 284-1 well and the transmission loss as a synthetic seismogram with a Ricker wavelet frequency of 14 Hz, zero-offset, and normal polarity. From the sonic and density logs (Figure 7), the reflection coefficient is calculated at SB 284-1 well, as well as the transmission loss of several varieties as: primary only (*P* only), primary with transmission loss (*P+TL*), primary with multiples (*P+M*), multiples only (*M* only) and primary with time-variant filter (*P* only+*TVF*). The positive values of the reflection coefficient may be due to the first that the acoustic impedance at the top of Zeit Formation is greater than that at the top of Post-Zeit Formation.

VELOCITY ANALYSIS

The first parameter considered in the seismic analysis is the seismic wave velocity. The accuracy of seismic data processing and interpretation depends mainly on the accuracy of velocity measurements. Velocity calculations, however, are based on the data obtained from drill-holes such as the continuous velocity survey (CVL). Velocity plays an essential role in the common-depth point (CDP) stacking, time migration, identification of multiples, time-depth conversion, modeling and compensation of amplitudes for the effect of geometrical spreading.

Accurate velocity determination requires not only the quality of travel time measurements, but also the choice of appropriate models for the actual geology and for the seismic process in [8]. Seismic velocities are subjected to variations both vertically and horizontally. The velocity of sound waves in rocks varies vertically with the compaction of rocks and with both the vertical and lateral lithologic changes. The compaction factor tends to increase the velocity with depth. However, the changes in lithology, (like a change from shale to carbonate) can produce an increase in velocity and in other cases (from carbonate to shale) a decrease as well in [9].

Analysis of the recorded data normally includes some details about the lateral and vertical continuity as an average and interval velocity map through several wells. The average and interval velocities have been computed and plotted *versus* the depths of the encountered formations.

Average Velocity Maps

The average velocity ($\overline{V}$) is the ratio of distance along a certain path to the time required for a wave to traverse the path, according to [6]:

$$\overline{V} = \left(\int_0^t V(t)\right) \mathrm{d}t \Big/ \int_0^t \mathrm{d}t . \tag{5}$$

The velocity data are measured from the sonic logs, normal moveout, well shooting and refraction time-distance curves. Four average velocity contour maps (Figure 8) for the four studied formations have been constructed. The average velocity

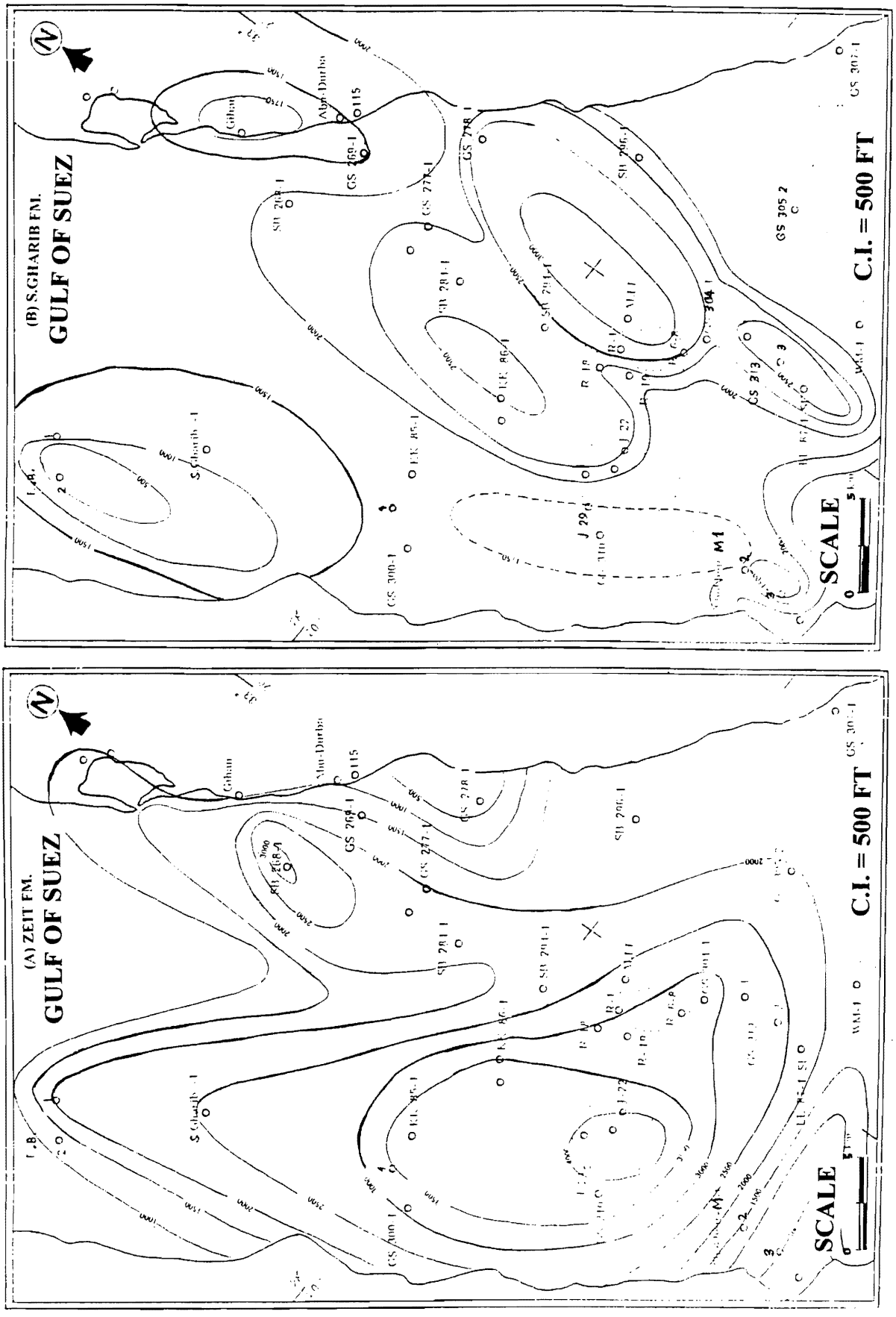
(B) S.GHARIB FM.
GULF OF SUEZ
C.I. = 500 FT
SCALE
(A) ZEIT FM.
GULF OF SUEZ
C.I. = 500 FT
SCALE

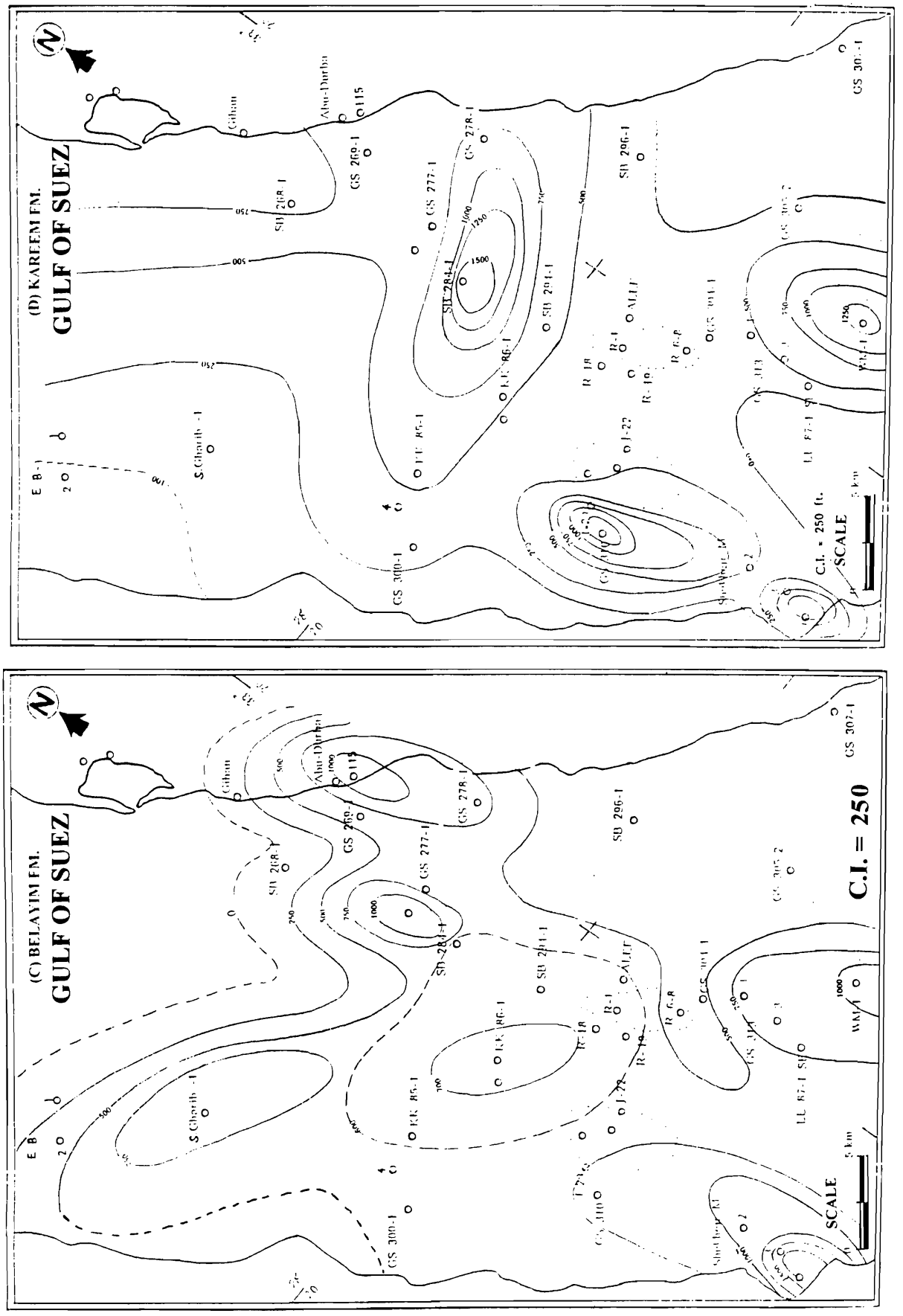

Figure 3. Isopach Map for Zeit Formation (A), South Gharib Formation (B), Belayim Formation (C), Kareem Formation (D).

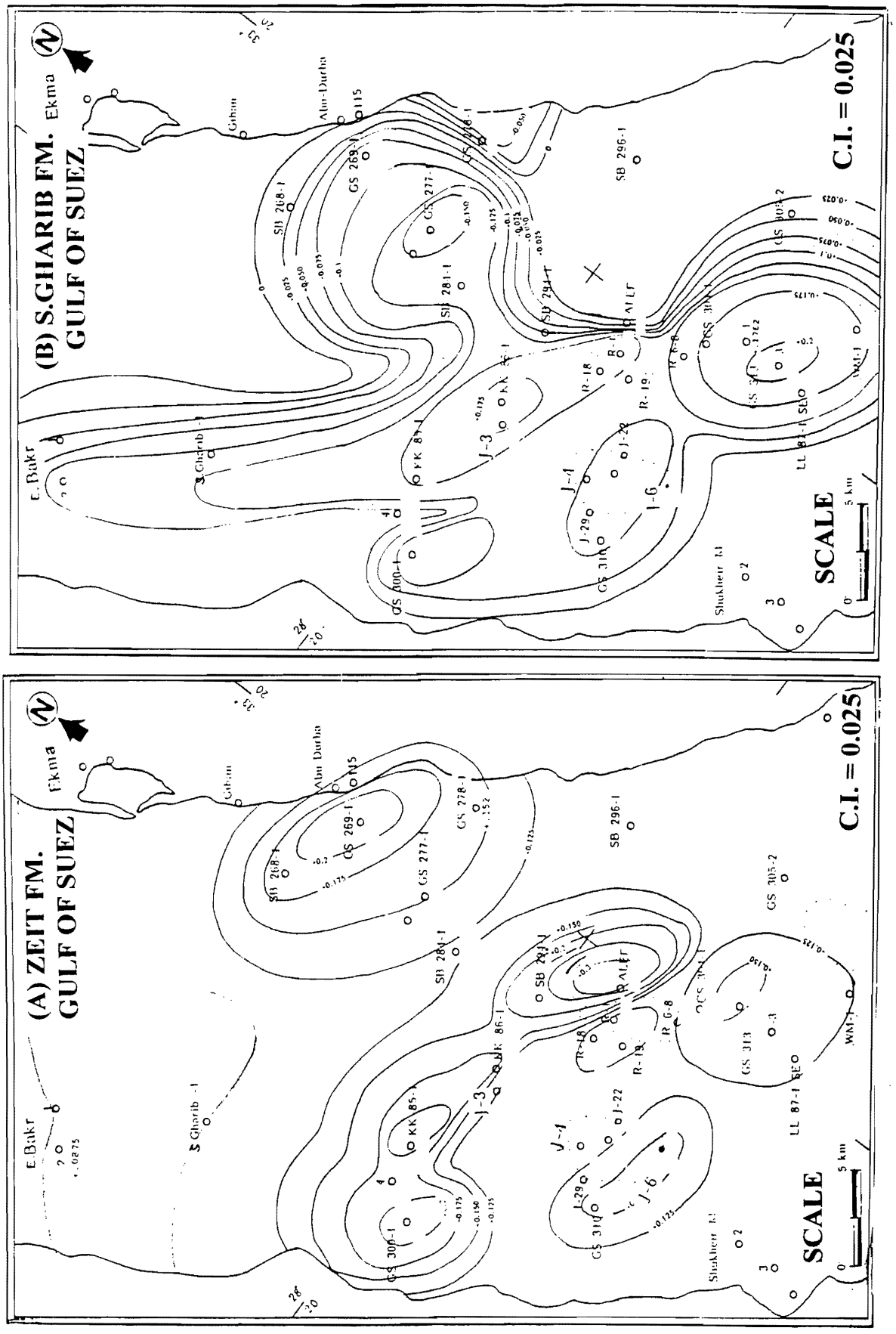
(A) ZEIT FM.
GULF OF SUEZ
C.I. = 0.025
SCALE
5 km
(B) S.GHARIB FM.
GULF OF SUEZ
C.I. = 0.025
SCALE
5 km

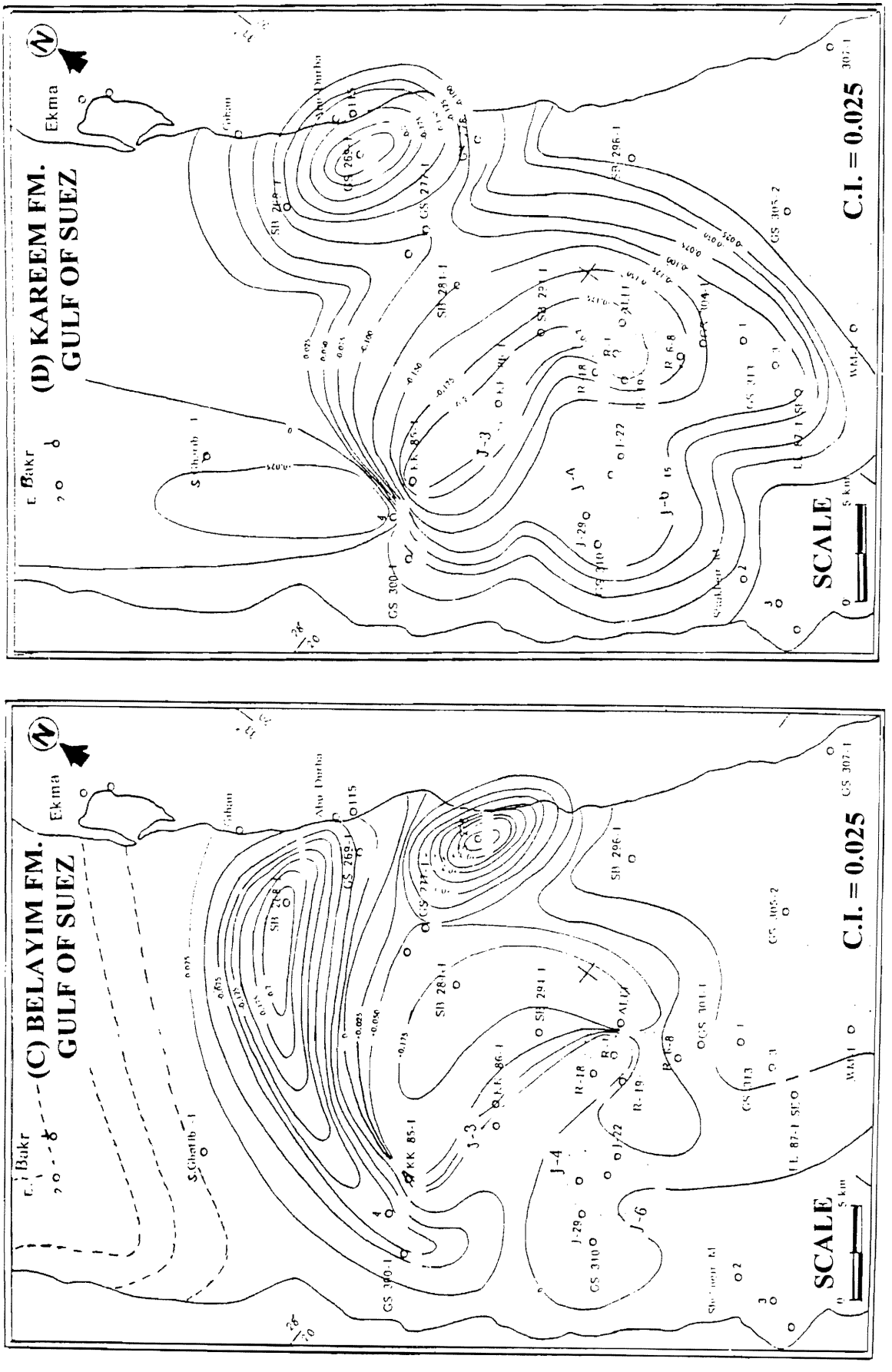

Figure 4. Reflection Coefficient Map on Top Zeit Formation (A), South Gharib Formation (B), Belayim Formation (C), Kareem Formation (D).

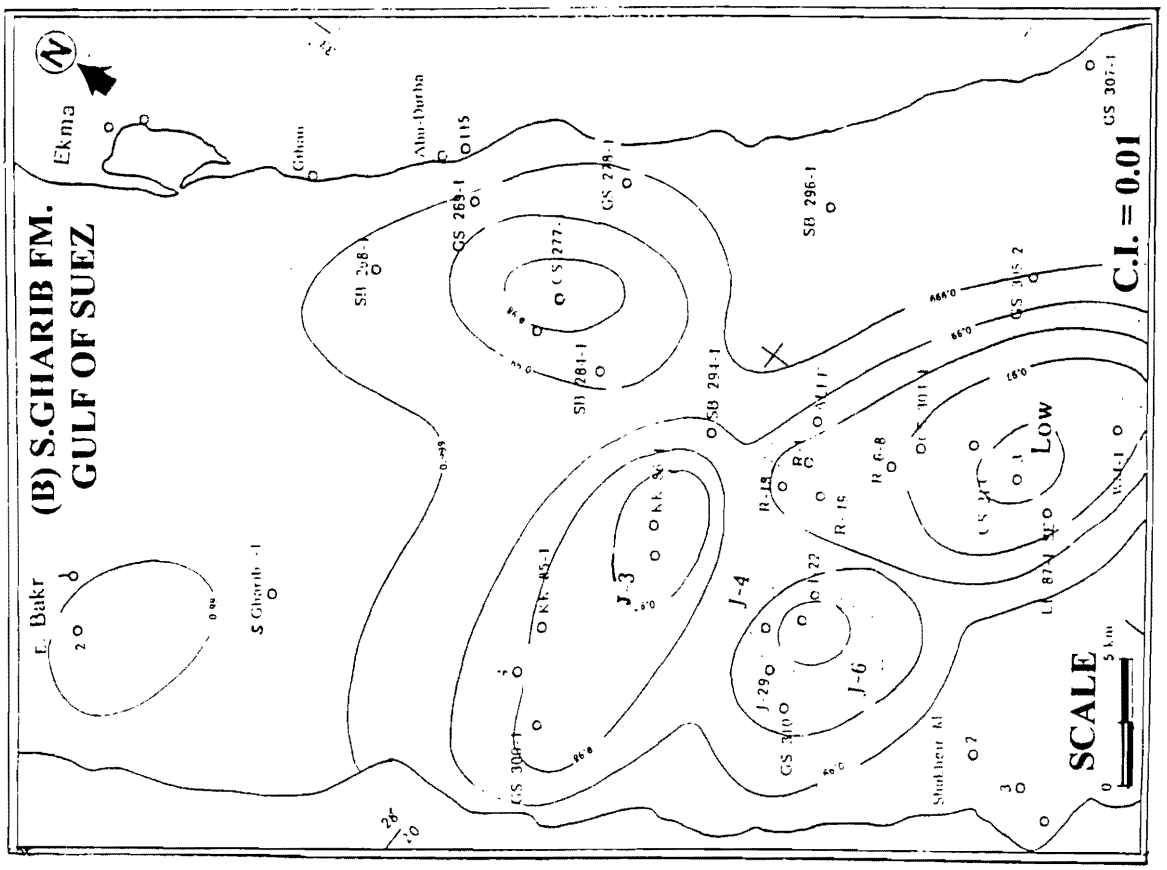
(B) S.GHARIB FM.
GULF OF SUEZ
E. Bakr
Ekma
Gharib
Abu Darba
SB 268-1
GS 269-1
GS 277-1
GS 278-1
SB 281-1
SB 284-1
SB 294-1
SB 296-1
GS 300-1
GS 305-2
GS 307-1
KK 85-1
J-3
J-4
J-6
J-29
GS 310
R-18
R-19
R 6-8
Low
SCALE
5 km
C.I. = 0.01

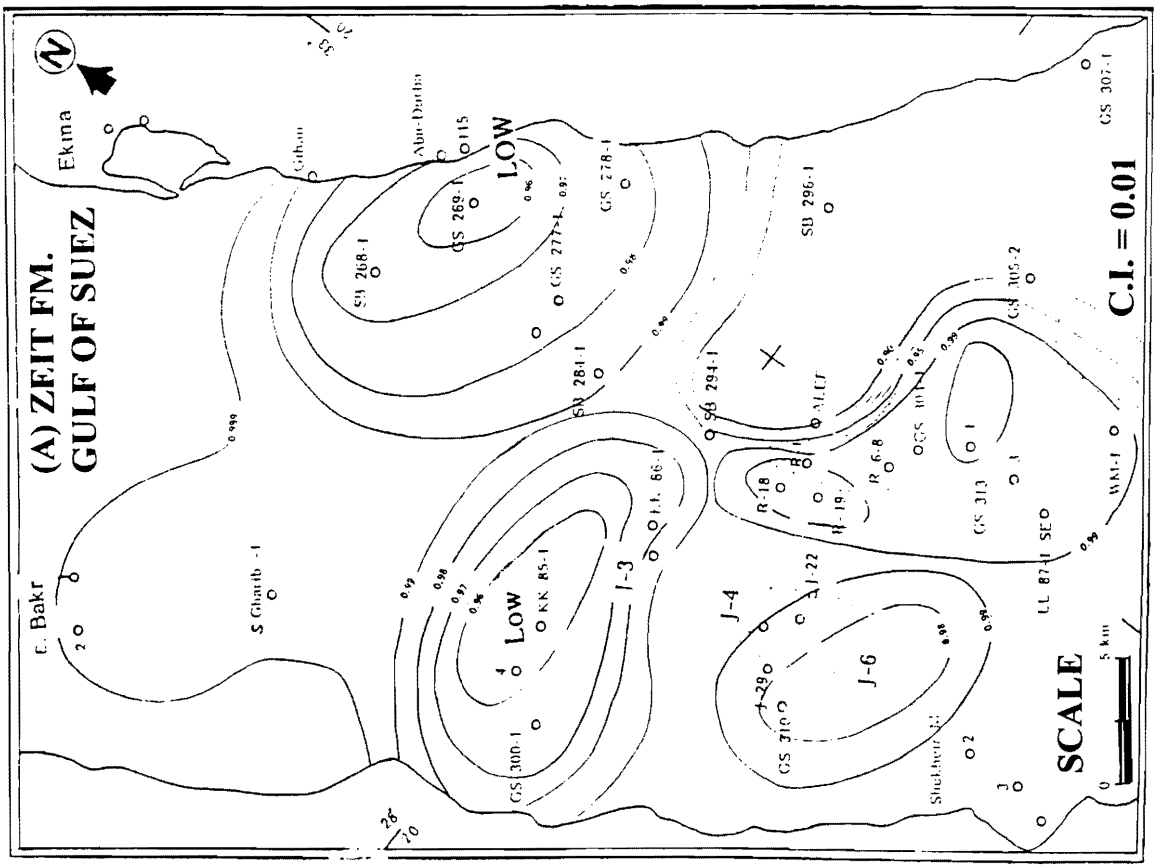
(A) ZEIT FM.
GULF OF SUEZ
E. Bakr
Ekma
Gharib
Abu Darba
LOW
SB 268-1
GS 269-1
GS 277-1
GS 278-1
SB 284-1
SB 294-1
SB 296-1
GS 300-1
GS 305-2
GS 307-1
KK 85-1
J-3
J-4
J-6
J-29
GS 310
R-18
R-19
R 6-8
SCALE
5 km
C.I. = 0.01

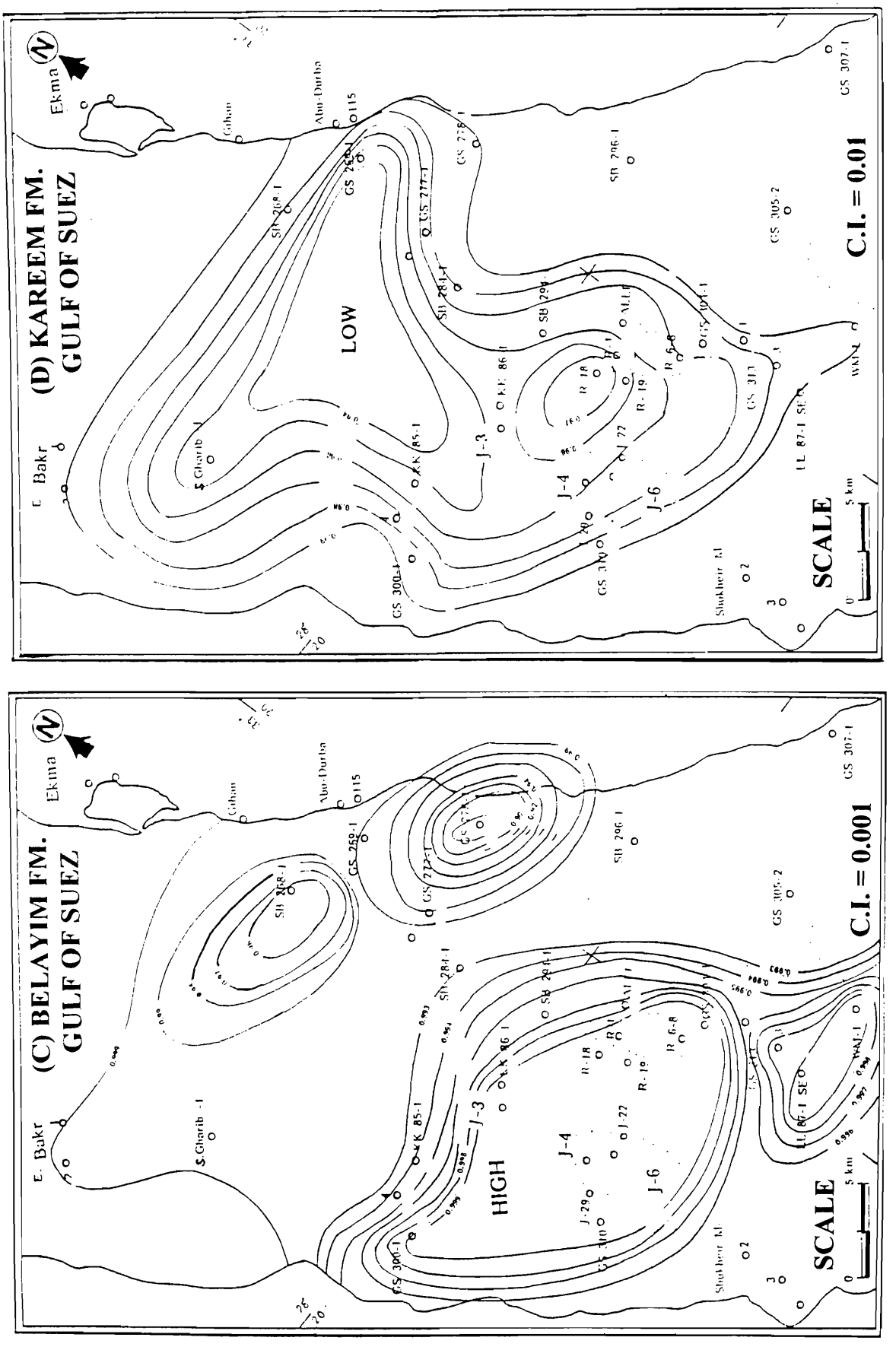

Figure 5. Transmission Coefficient Map on Top Zeit Formation (A), South Gharib Formation (B), Belayim Formation (C), Kareem Formation (D).

map to the top of Zeit Formation (Figure 8*a*) shows an observable increase of velocity in the eastern portion at GS 269-1 and GS 278-1 wells and a decrease of velocity in the central and western portions at GS 313-1 and GS 300-1 wells. High velocity may be attributed to massive rocks (evaporites), while low velocity to loose sediments (shale). Figure (8*b*) represents the variations of average velocity to the top of South Gharib Formation. It shows an increase of the average velocity in the central part at Alef-1 well and a decrease in the eastern and western portions. The average velocity varies from 10 699 ft/sec at Alef-1 well to 8294 ft/sec at GS 278-1 well. This depends mainly on the variations in lithology.

The average velocity map to the top of Belayim Formation (Figure 8*c*) shows an increase toward the central portion of 11 823 ft/sec at Alef-1 well and then decreases until it reaches the coastal lines with 9164 ft/sec at E. Baker M-1 well. The average velocity map to the top of Kareem Formation (Figure 8*d*) shows a maximum value at the central portion (of 12 050 ft/sec in Alef-1 well) and then decreases in all directions. The average velocity maps are used to convert the subsea depths of all wells into two-way travel time to verify the well ties with the seismic sections and also to convert the reflection time maps into depth maps.

Interval Velocity Maps

The interval velocity is the average velocity over some intervals of the travel path. It is often calculated from stacking velocities for the interval between the reflectors. It is computed from the root-mean square (RMS) velocities through [10] equation and is given approximately by the relation:

$$V_{INT} = \left(\frac{V_b^2 T_b - V_a^2 T_a}{T_b - T_a} \right)^{1/2} \tag{6}$$

where: V_a and V_b are the RMS velocities at the top and bottom of the interval, respectively. Also, T_a and T_b are the zero-offset two-way arrival times at the top and bottom of the same interval, respectively. For isotropic horizontal layers, $V_{NMO} = V_{rms}$, where V_{NMO} is the normal-moveout velocity. Rms velocities are typically a few percent larger than the corresponding average velocities.

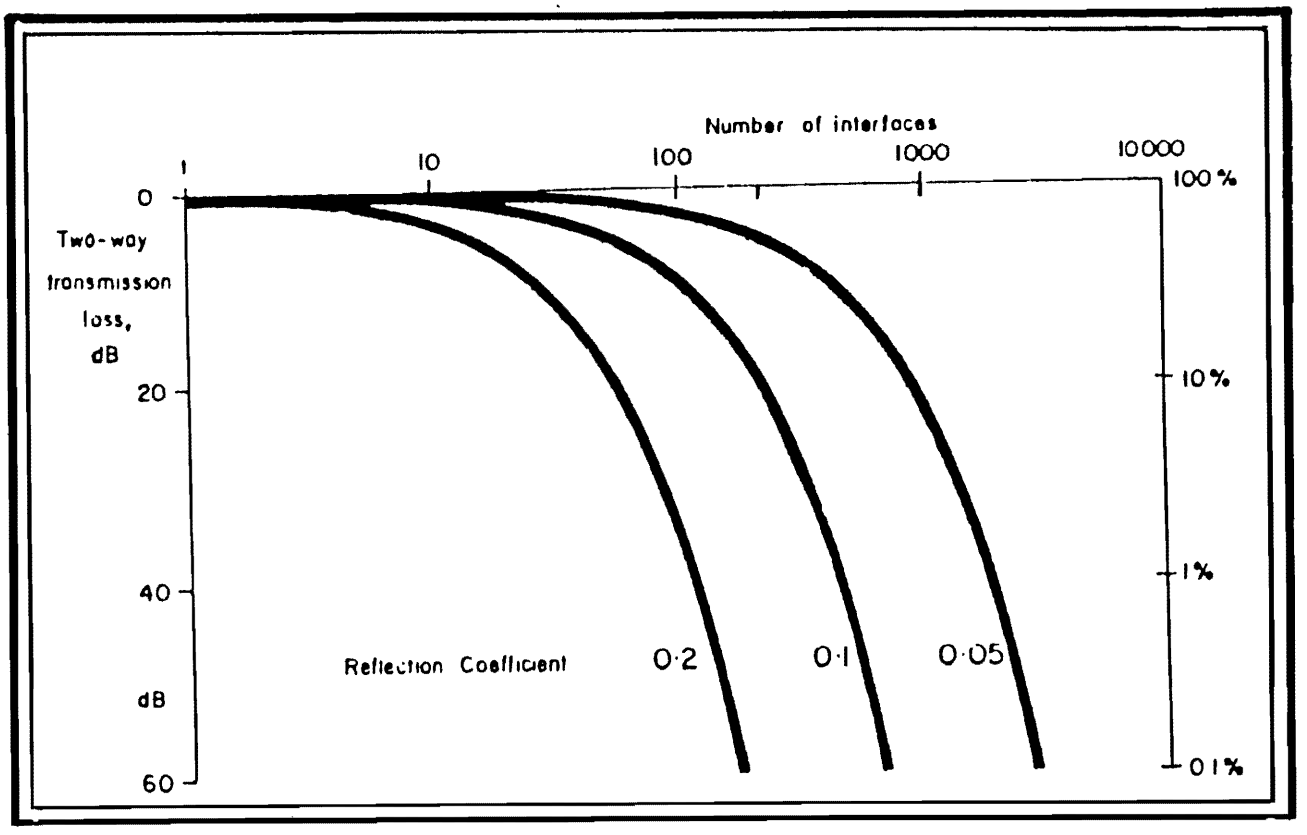

Figure 6. Two-Way Transmission Loss Through a Number of Interfaces, for a Range of Reflection Coefficients (after O'Doherty and Anstey [7].

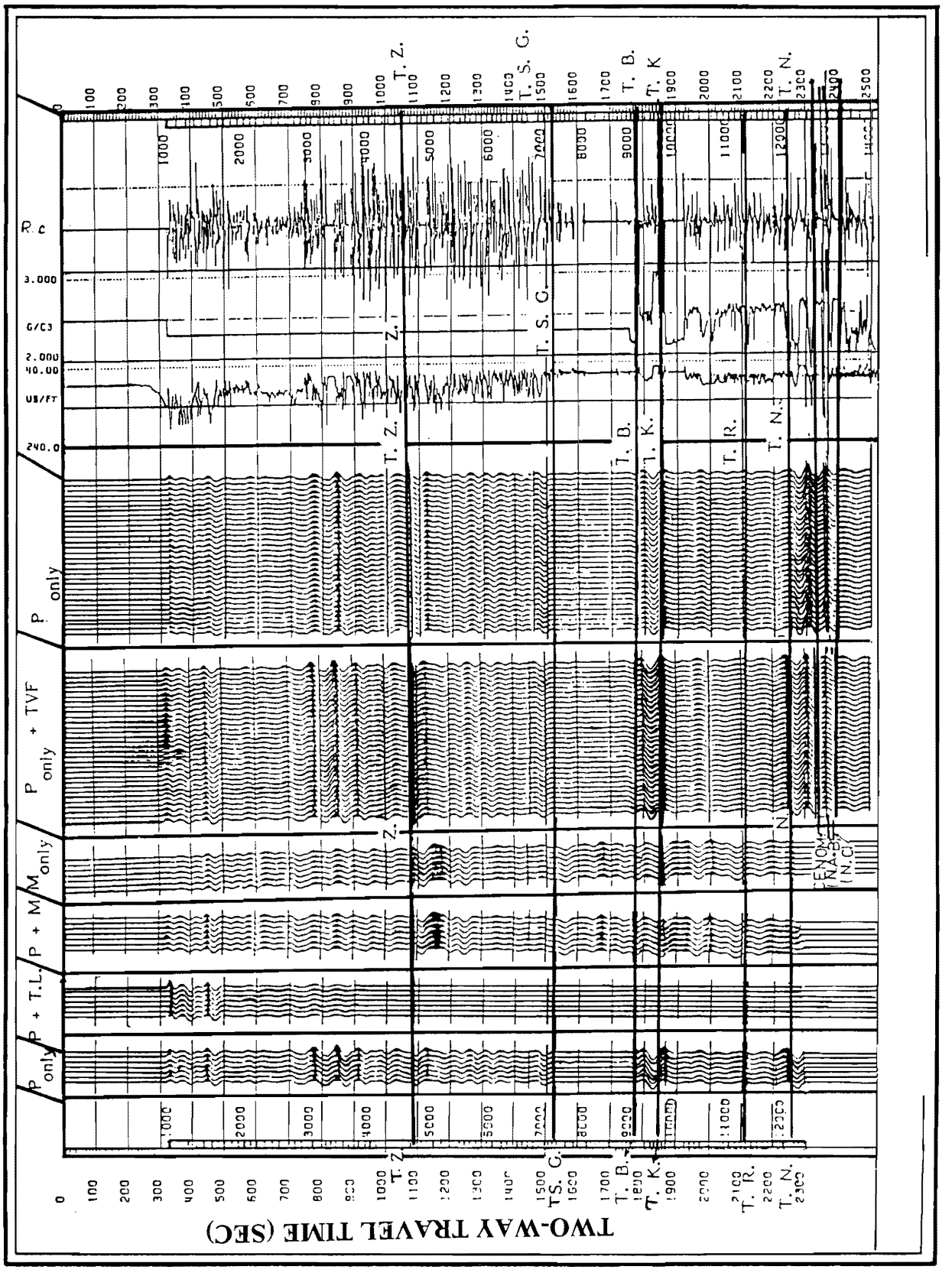

Figure 7. Synthetic Seismogram for the Well SB 284-1, Wavelet Frequency = 14 Hz, Zero Offset, Normal Polarity, South Belayim Area, Gulf of Suez.

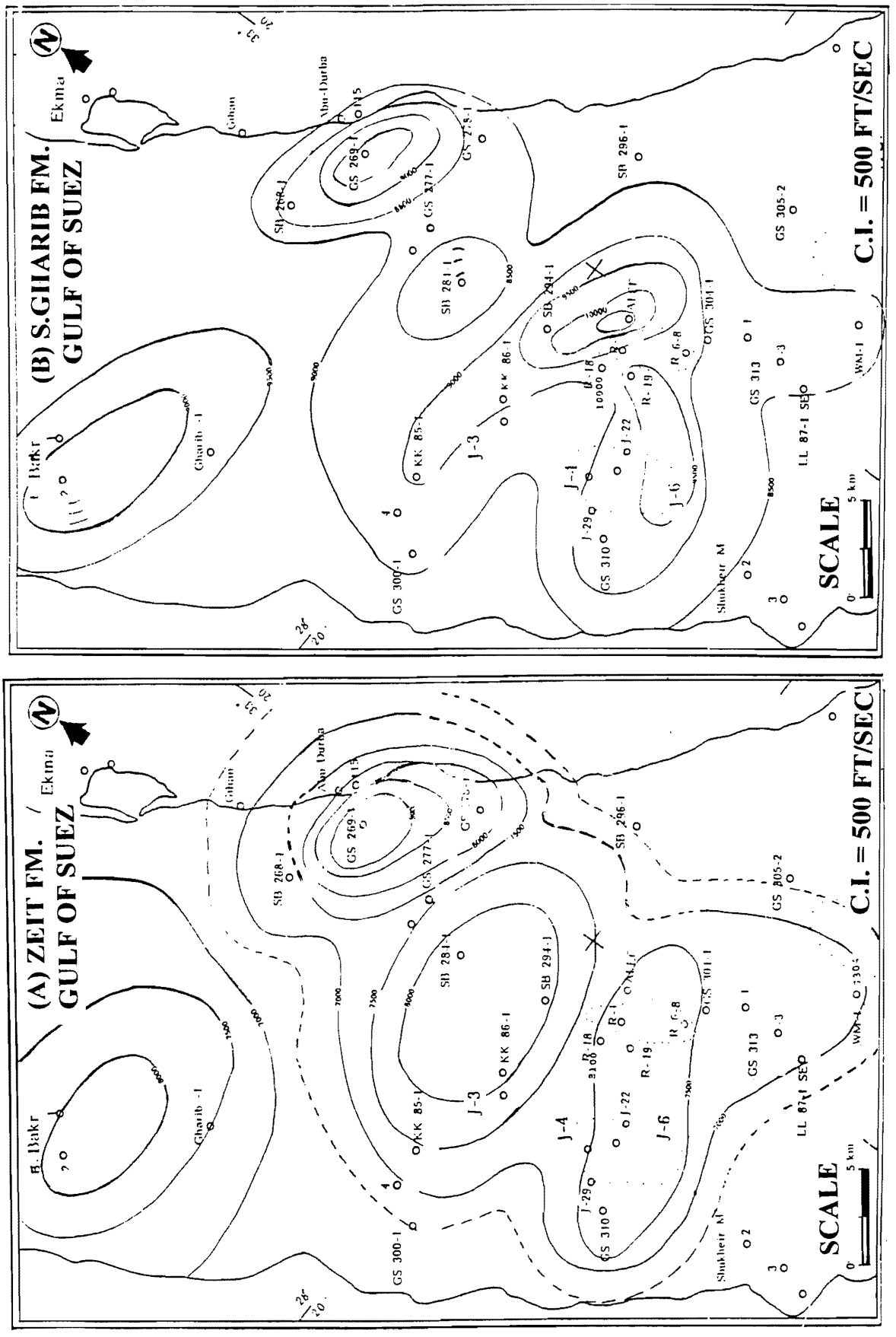
(A) ZEIT FM.
GULF OF SUEZ
(B) S.GHARIB FM.
GULF OF SUEZ
C.I. = 500 FT/SEC
SCALE
5 km
Ekma
Gharib -1
Abu Durba
Geban
SB 268-1
GS 269-1
GS 277-1
SB 281-1
SB 294-1
SB 296-1
KK 86-1
KK 85-1
J-1
J-3
J-4
J-6
J-22
J-29
GS 310
GS 300-1
GS 313
GS 305-2
LL 87-1 SEO
WM-1
Shukheir M

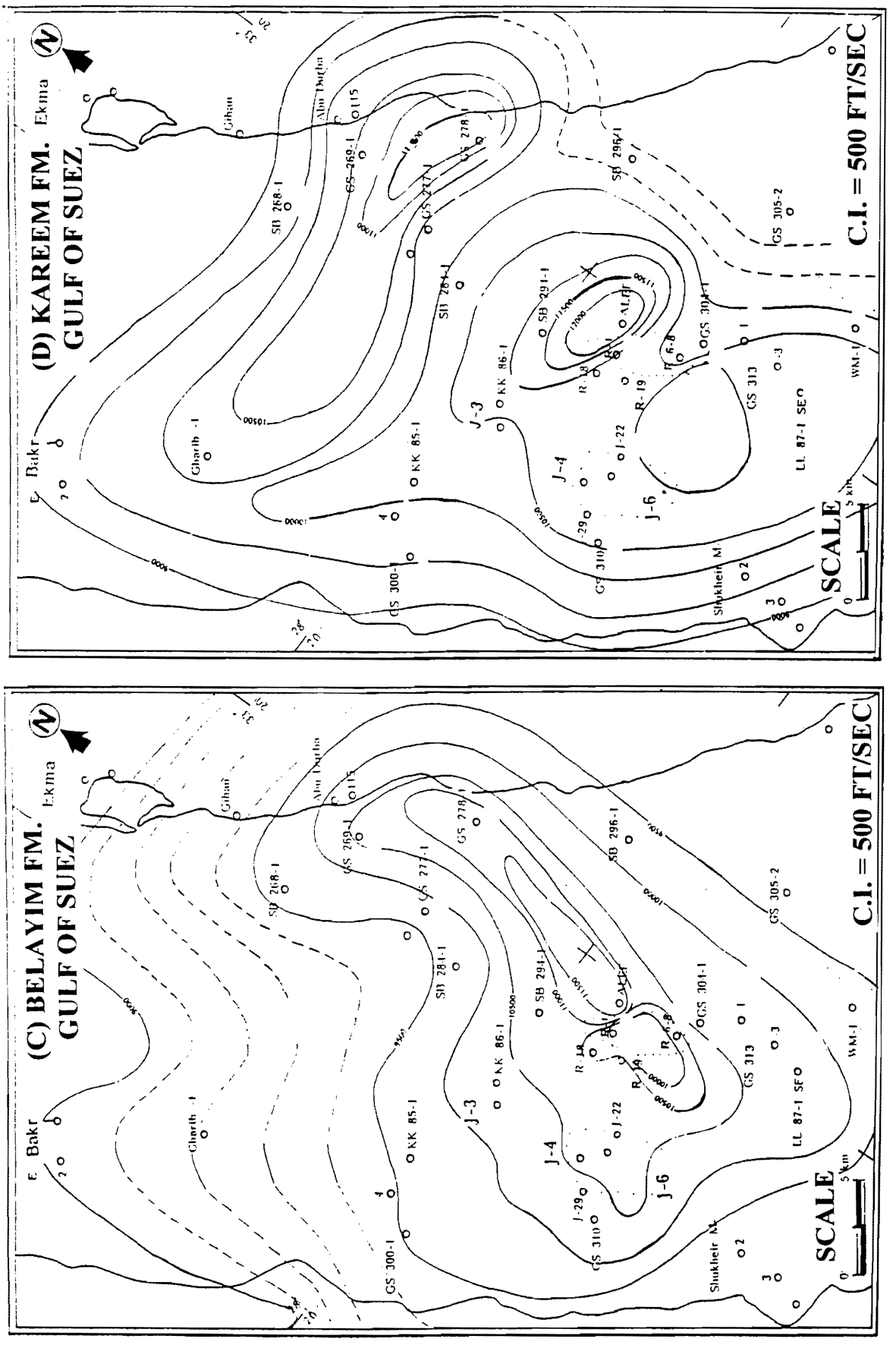

Figure 8. Average Velocity Map from the Surface to the Top of Zeit Formation (A), South Gharib Formation (B), Belayim Formation (C), Kareem Formation (D).

Four interval velocity contour maps (Figure 9) of the four evaluated formations have been constructed. The interval velocity maps of the Zeit and South Gharib Formations (Figure 9*a* and *b*) show small values in the Zeit Formation and large values in the South Gharib Formation. This is due to the variations in the lithology of these two formations. Zeit Formation is formed essentially of cyclic layers of shale and anhydrite, while South Gharib Formation is mainly salt. The large interval velocity values of Belayim Formation (Figure 9*c*) are related to the non-clastic rock unit, but in Kareem Formation (Figure 9*d*) the interval velocity values are intermediate due to intercalation between marls and shales with sandstones.

Consequently, this area can be subdivided into six depositional basins trending in the NW-direction (*e.g.* northern part, SB 296-1, block-300, Ramadan, July, and Shukeir). The velocity anomalies appeared to be structurally controlled and are caused by the sound waves going through the salts, reefs, igneous dikes, and distorted beds. It is possible to identify the sources of these anomalies and to predict the distortion of the recognized reflectors. In some cases, the velocity data are enough for the establishment of a corrected section.

THE DISCORDANCE BETWEEN STACKING VELOCITIES AND CHECK-SHOT VELOCITIES

The difference between stacking velocities and average velocities, deduced from check shot surveys, is discussed in [11]. The check shooting was done with an airgun source close to the well head. The check shooting represents approximately a vertical path, while the stacking velocities represent slant ray paths. Stacking velocity (V_s) is the value used for the common-midpoint stacking in [6]. Between the drilled wells we have to use the root mean square velocity, as the measured average velocities are not normally available in [12].

The difference between stacking and NMO velocities is sometimes called spread-length bias [8]. Accordingly, the discordance is due to the geometrical raypaths [11]. Even if the velocity gather is centered on the well, the derived stacking velocity requires several corrections before representing it as an approximate average velocity. The stacking velocity is also subjected to significant errors in the presence of lateral changes of the interval velocity, such as those associated with the presence of hydrocarbons in the vicinity of the borehole in [11].

The CDP-derived velocities usually yield depth estimation errors that are a manifestation of the stacking velocity being different from the well log velocity in [13]. The stacking velocities are subject to more geometric problems than the check-shot velocities, such as lensing, blind spots, and the effects of dip and refraction. Generally, the consequences of the wavefront healing are also different. Abu El-Ata [14] mentioned that the root mean square velocity equals the average velocity when the layer is homogeneous and progressively exceeds it when the latter becomes more heterogeneous.

Since the check-shooting represents a one-way path, the effects of absorption *versus* multiples and scattering are less marked. The velocities actually using a conventional CDP velocity analysis are created from horizontal velocity in [15]. In the presence of anisotropy, the stacking velocity deviates from the check-shot velocity. Most of the above considerations are in favor of the check-shot velocities over the stacking velocities. However, the stacking velocities cannot be expected to be equal to the check-shot velocities unless proper attention is paid to the corrections and to the place of the pulse which is selected for picking.

Discordance Maps for Average Velocity

The discordance map for the average velocity to the top of Zeit Formation (Figure 10*a*) reflects the zero line passing through several wells (GS 278-1, J-3, KK 86-1, Alef-1, R1-21, GS 304-1, and GS 313-1). This line indicates that, the average velocity in the check-shot survey is probably equal to the stacking velocity. But this is not correct for several reasons such as: NMO corrections, spherical divergence, high noises and strong multiples in the stacking velocity. So, it is impossible to know the accurate zero line. It could be present with a small difference (plus or minus) between the two types of velocities. In the case of positive values, the check-shot velocity is larger than the stacking velocity and vice versa.

The eastern part has positive values of (+2%) indicating that the velocity analysis in the processing sequence is accurate in this area. At the central part, negative values (−16% at GS 277-1 well) are estimated. This means that wrong stacking velocities were selected and should be corrected in the velocity analysis. Figure (10*b*) shows the discordance map for average velocity of the South Gharib Formation. A positive value of +11% is observed at Alef-1 well. The other wells have negative values, the maximum values are −18% and −17% at GS 304-1 and GS 277-1 wells, respectively.

The discordance map for average velocity to the top of Belayim Formation (Figure 10*c*) shows positive values at the eastern part in GS 278-1 (+12%) and Alef-1 (+7%) wells, while other wells display negative values with the maximum value of (−16.5 %) at GS 277-1 well. Figure (10*d*) shows the discordance map for average velocity to the top of Kareem

Formation. The positive values at GS 278-1 and Alef-1 wells +10.6% and +6.6% are calculated, respectively and the other wells have negative values with a maximum value of (–17%) at SB 268-1 well.

Discordance Maps for Interval Velocity

Figure (11*a*) shows the discordance map for the interval velocity of Zeit Formation, where two wells have positive values: SB-268-1 (+39.7%) and GS 269-1 (+12.5%), and the other wells have negative values (the maximum value is –33% at GS 278-1 well). It can be noticed that the northern part has negative values, while the central part exhibits positive values. Figure (11*b*) shows the discordance map for the interval velocity of South Gharib Formation, that ranges from +28.6% at GS 278-1 well to –17.3% at GS 304-1 well.

Figure (11*c*) exhibits the discordance map for the interval velocity of Belayim Formation which has positive values except at GS 277-1 (–5%) and GS 304-1 (–17%) wells. These positive values are ranging from +19% (at J-3 well) to +1% (at GS 313-1 well). Two lines of zero value have been detected, one in the eastern side around the wells: GS 269-1 (positive value) and GS 277-1 (negative value) and the others between the wells (J-3 and KK 86-1A) and (R1-21 and Alef-1). The negative values range from –33% at GS 313-1 well to –1% at J-3 well, while the positive values range from +50% at SB 268-1 well (the largest error value) and +12% at KK 86-1A well.

Figure (11*d*) shows the discordance map for the interval velocity of Kareem Formation. The zero line runs from the central part towards the NE direction passing through the negative values that range from –56% at GS 269-1 well to –2% at Alef-1 well. Only a single positive value at SB 268-1 well (+4%) is calculated. The wells are usually drilled in the locations of structural highs, where significant variations in the velocity can be predicted close to the hole.

VELOCITY GRADIENT MAPS

Evaluation of the velocity function at each well location has been performed. The relation between velocity and its depth is a linear relation calculated for the 24 studied wells (Table 1):

$$V = V_0 + KZ, \tag{7}$$

where: V is the instantaneous velocity at the vertical depth Z, V_0 is the intercept velocity at datum, and K is the velocity gradient. The values of V_0 and K were obtained at each well location by least squares linear fitting of the average velocity with depth relation to the top of the Kareem Formation.

The velocity gradient contour (K) map (Figure 12) shows a minimum value of 0.39 for the K at the central part of the gulf at KK 86-1, KK 85-1, J-4, and R-19 wells. But, it increases in all directions until it reaches a value of 1.007 at GS 278-1 well. In Figure 13, the intercept velocity contour (V_0) map at the datum of top Kareem Formation shows a maximum value of (V_0) in the central part at KK 86-1 well to give 7408 ft/sec. This value decreases in all directions until it reaches 5260 ft/sec at SB 268-1 well. At GS 269-1 well it gives a maximum value of 7722 ft/sec as an exceptional case, because it

Table 1. Values of V_0 [ft/sec] and K of the 24 Wells, Used in The Area Studied.

No.	Wells	K	V_0	No.	Wells	K	V_0
1	R-1	0.46	6864	13	GS 269-1	0.39	7722
2	R-18 A	0.42	6808	14	SB 284-1	0.41	6240
3	GS 313-3	0.55	6700	15	GS 278-1	1.007	6291
4	GS 313-1	0.57	6502	16	KK 85-1	0.39	6801
5	LL 87 SE-1	0.55	6812	17	KK 86-1	0.38	7408
6	J-29	0.43	6980	18	R 6-8 A	0.40	7301
7	J-4	0.39	7179	19	R-5 A	0.42	7065
8	GS 277-1	0.46	5973	20	GS 304-1	0.49	6839
9	SB 268-1	0.43	5260	21	Alef-1	0.679	7427
10	J-3	0.43	6794	22	R-19 A	0.39	7017
11	J-22	0.41	7097	23	GS 300-1 A	0.73	5863
12	GS 310-1 B	0.45	6751	24	GS 300-4	0.63	6055

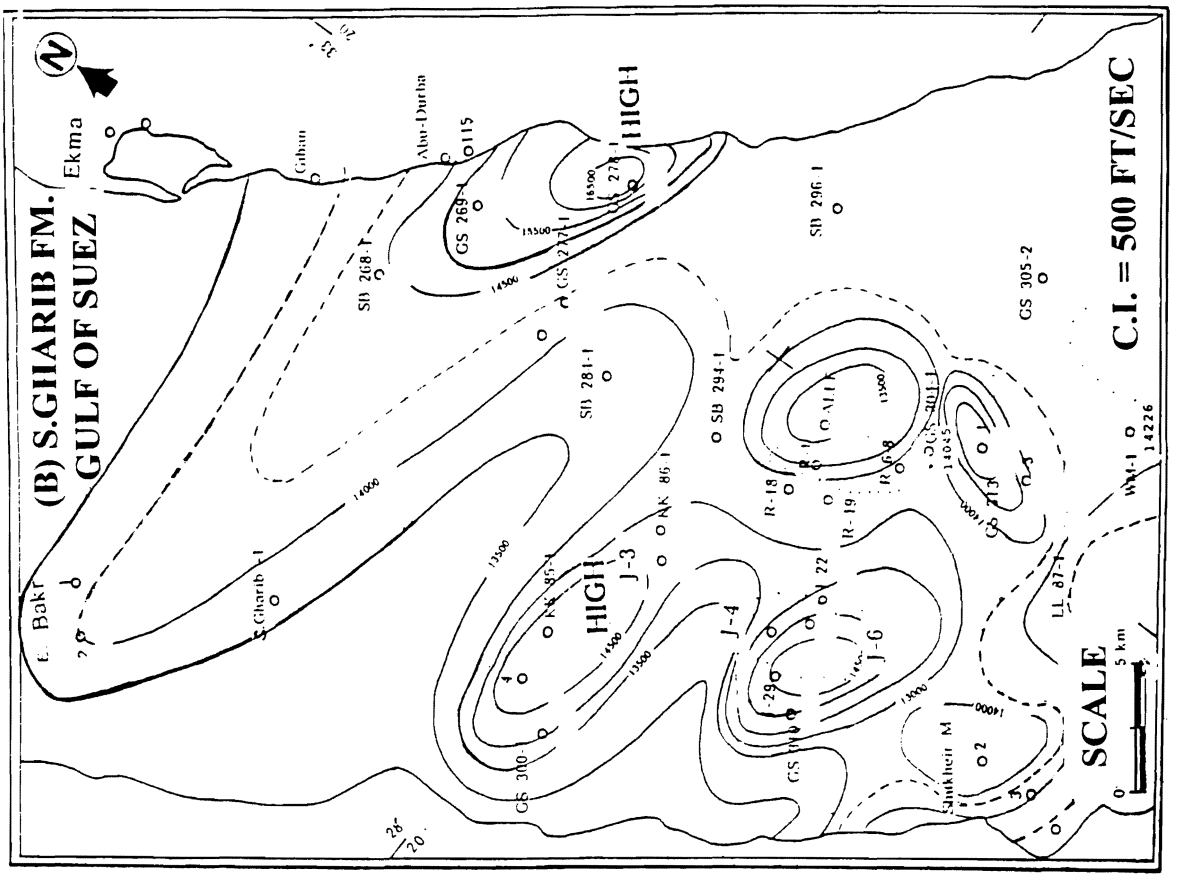
(B) S.GHARIB FM.
GULF OF SUEZ
Ekma
Gebun
Abu-Durba
E. Bakr
S.Gharib-1
HIGH
J-3
J-4
J-6
SCALE
C.I. = 500 FT/SEC

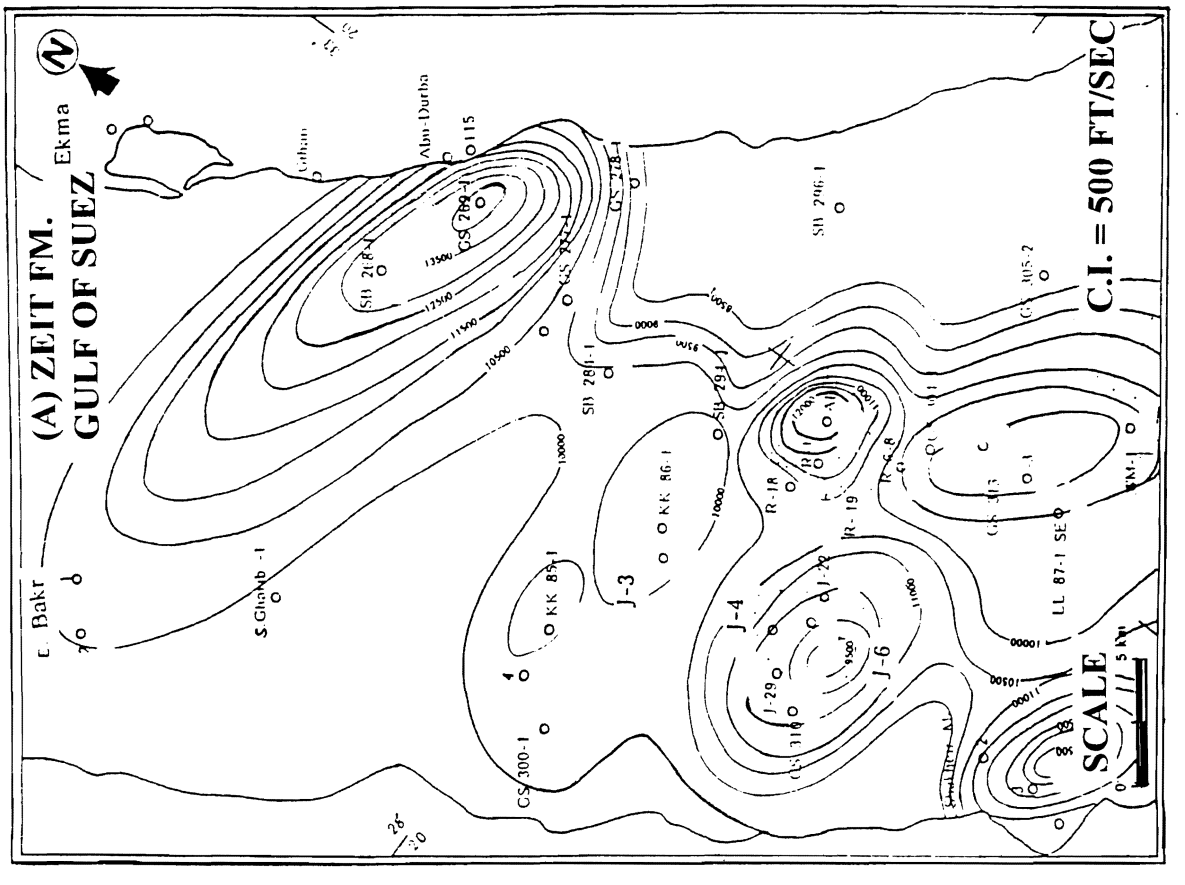
(A) ZEIT FM.
GULF OF SUEZ
Ekma
Gebun
Abu-Durba
E. Bakr
S.Gharib-1
J-3
J-4
J-6
SCALE
C.I. = 500 FT/SEC

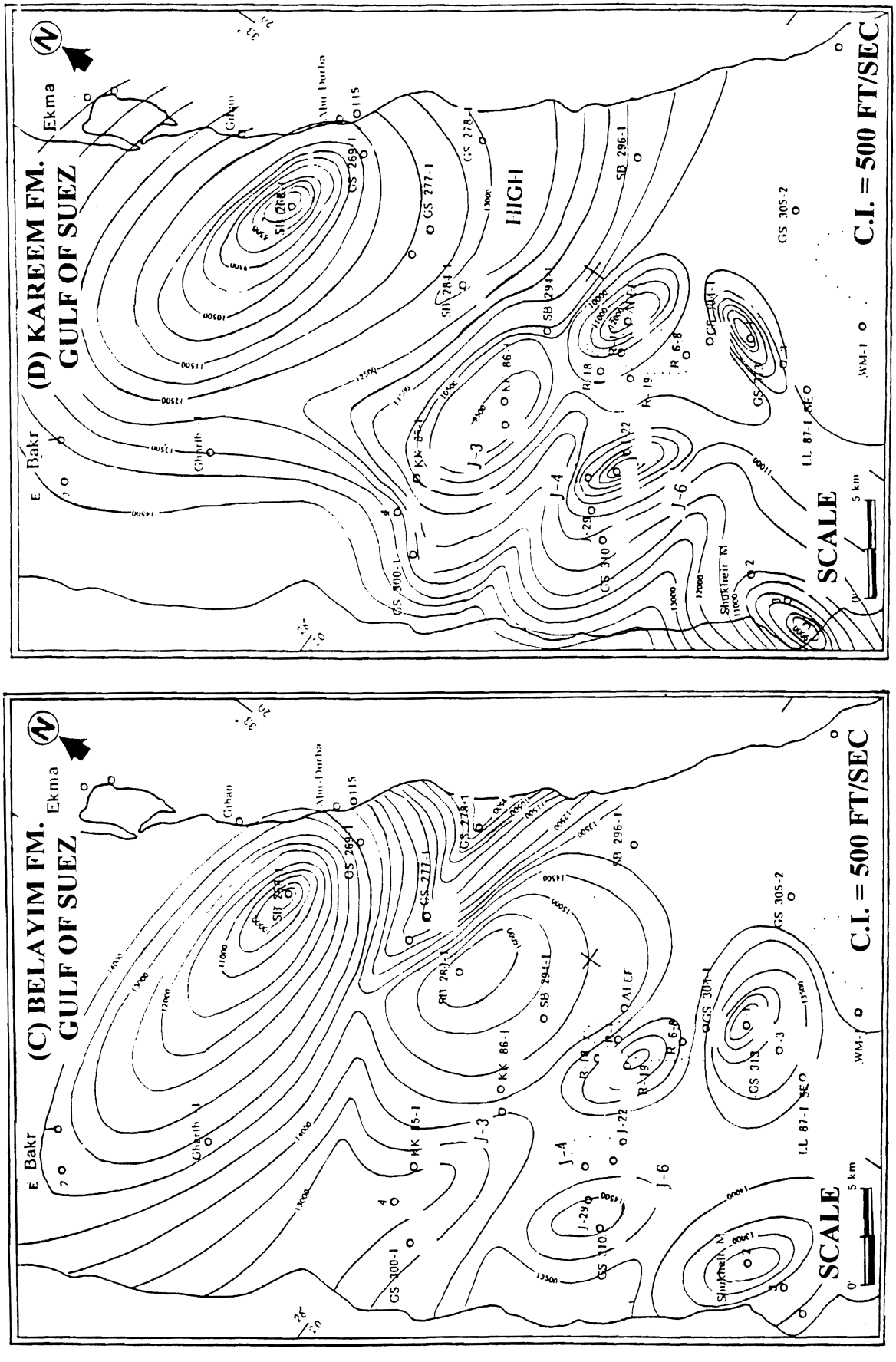

Figure 9. Interval Velocity Map of Zeit Formation (A), South Gharib Formation (B), Belayim Formation (C), Kareem Formation (D).

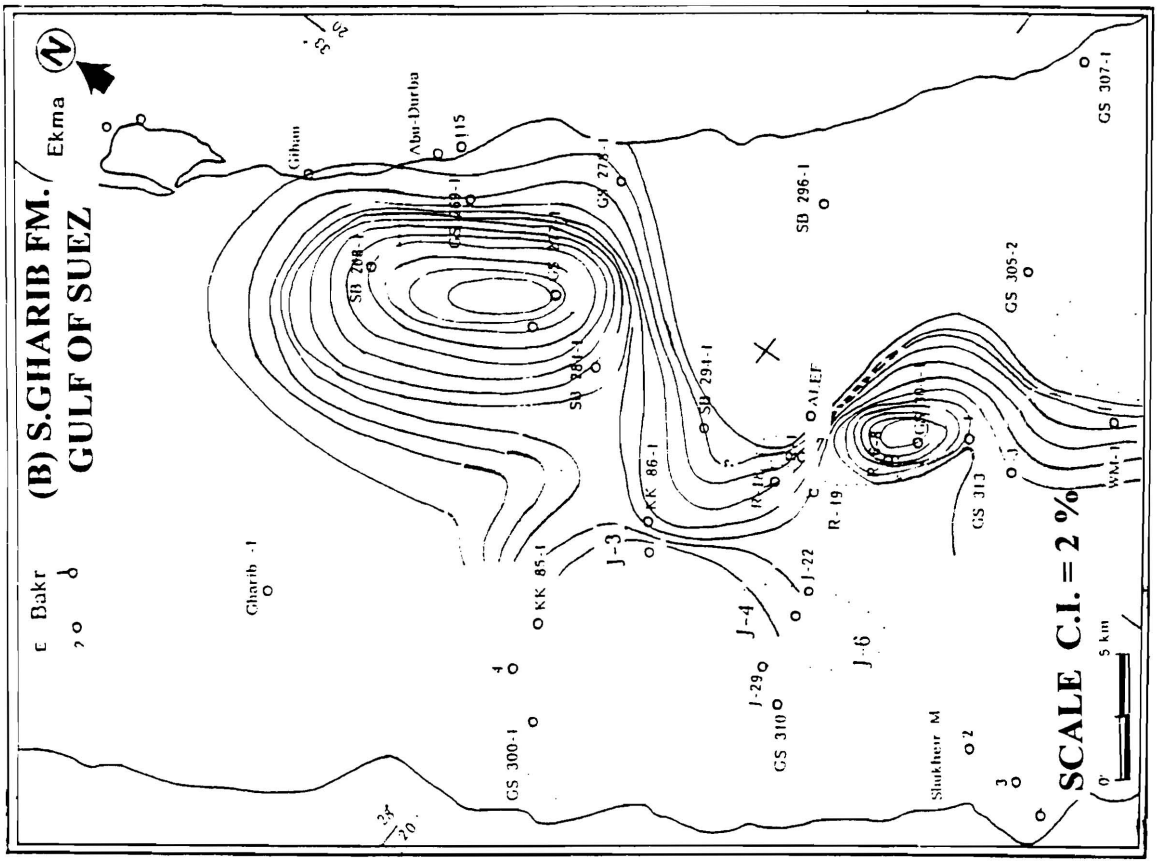
(B) S.GHARIB FM.
GULF OF SUEZ
Ekma
Gihan
Abu-Durba
115
GS 278-1
SB 296-1
GS 305-2
GS 307-1
SB 294-1
KK 86-1
KK 85-1
J-3
J-4
J-6
J-22
J-29
R-19
GS 300-1
GS 310
GS 313
WM-1
SCALE C.I. = 2 %
0
5 km

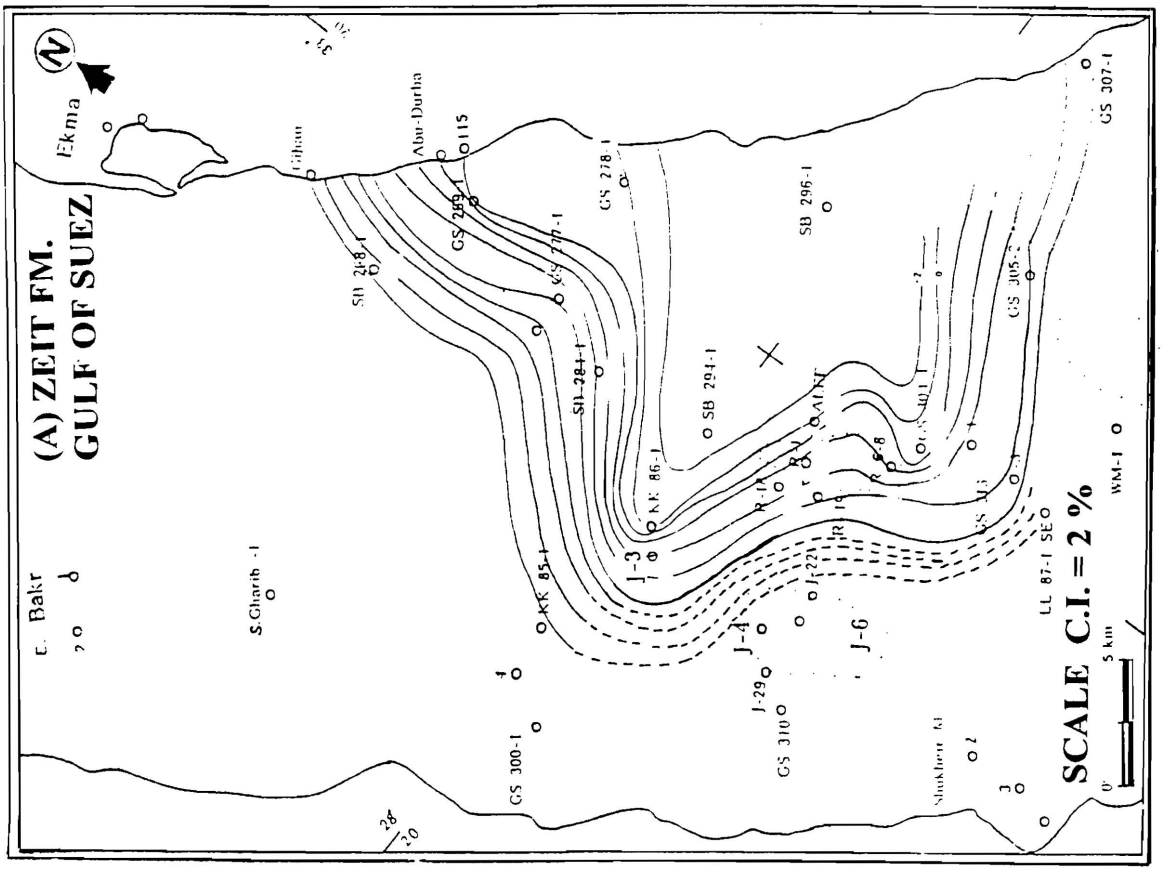
(A) ZEIT FM.
GULF OF SUEZ
Ekma
Gihan
Abu-Durba
115
GS 278-1
SB 296-1
GS 305-2
GS 307-1
SB 294-1
KK 86-1
KK 85-1
J-3
J-4
J-6
J-22
J-29
R-19
GS 300-1
GS 310
GS 313
WM-1
LL 87-1 SE
SCALE C.I. = 2 %
0
5 km

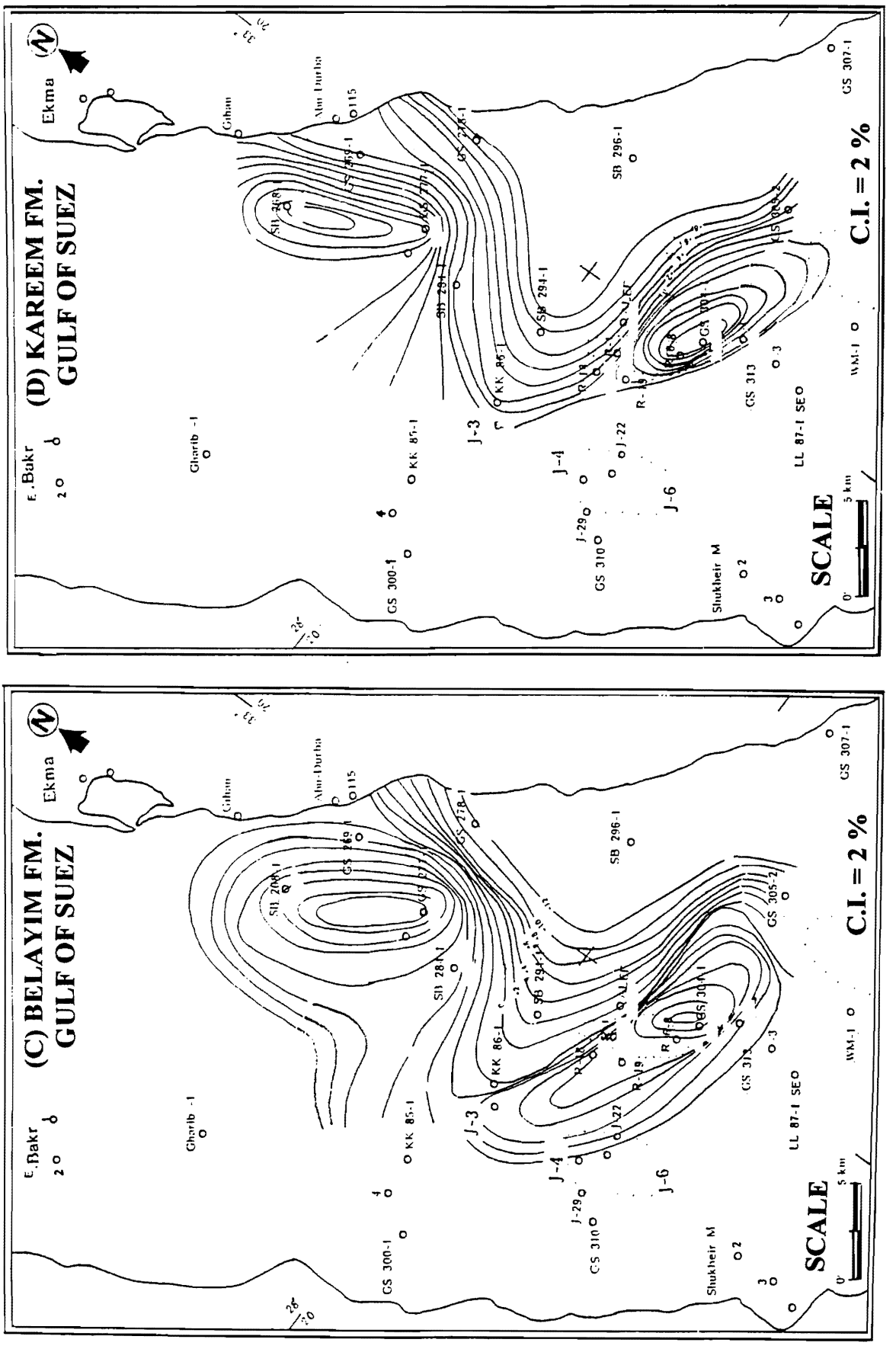

Figure 10. Discordance Map for Average Velocity from the Surface to the Top of Zeit Formation (A), South Gharib Formation (B), Belayim Formation (C), Kareem Formation (D).

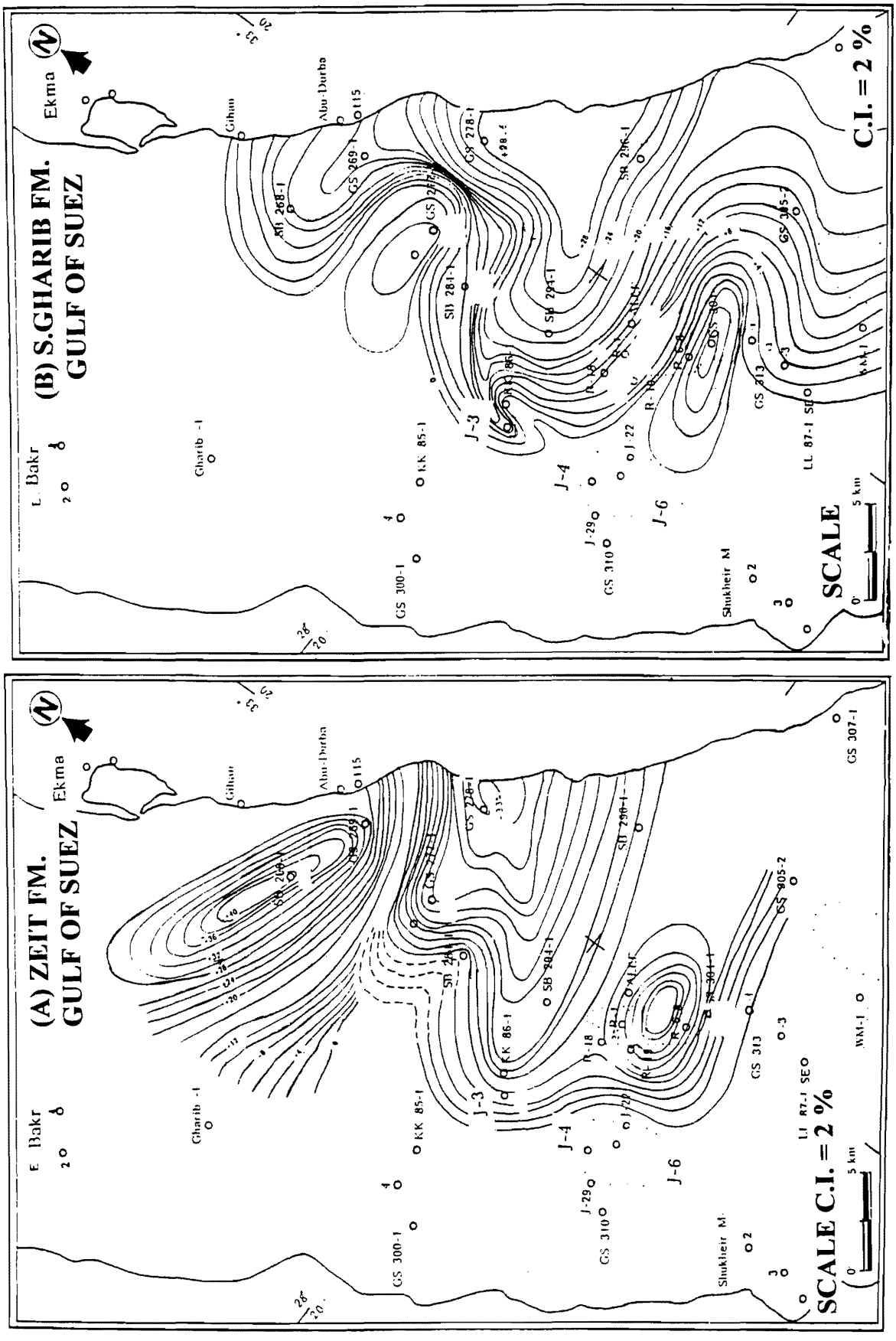
(A) ZEIT FM.
GULF OF SUEZ
(B) S.GHARIB FM.
GULF OF SUEZ
Ekma
Gharib -1
Abu-Durba
Shukheir M.
J-3
J-4
J-6
SCALE C.I. = 2 %
C.I. = 2 %
SCALE
5 km

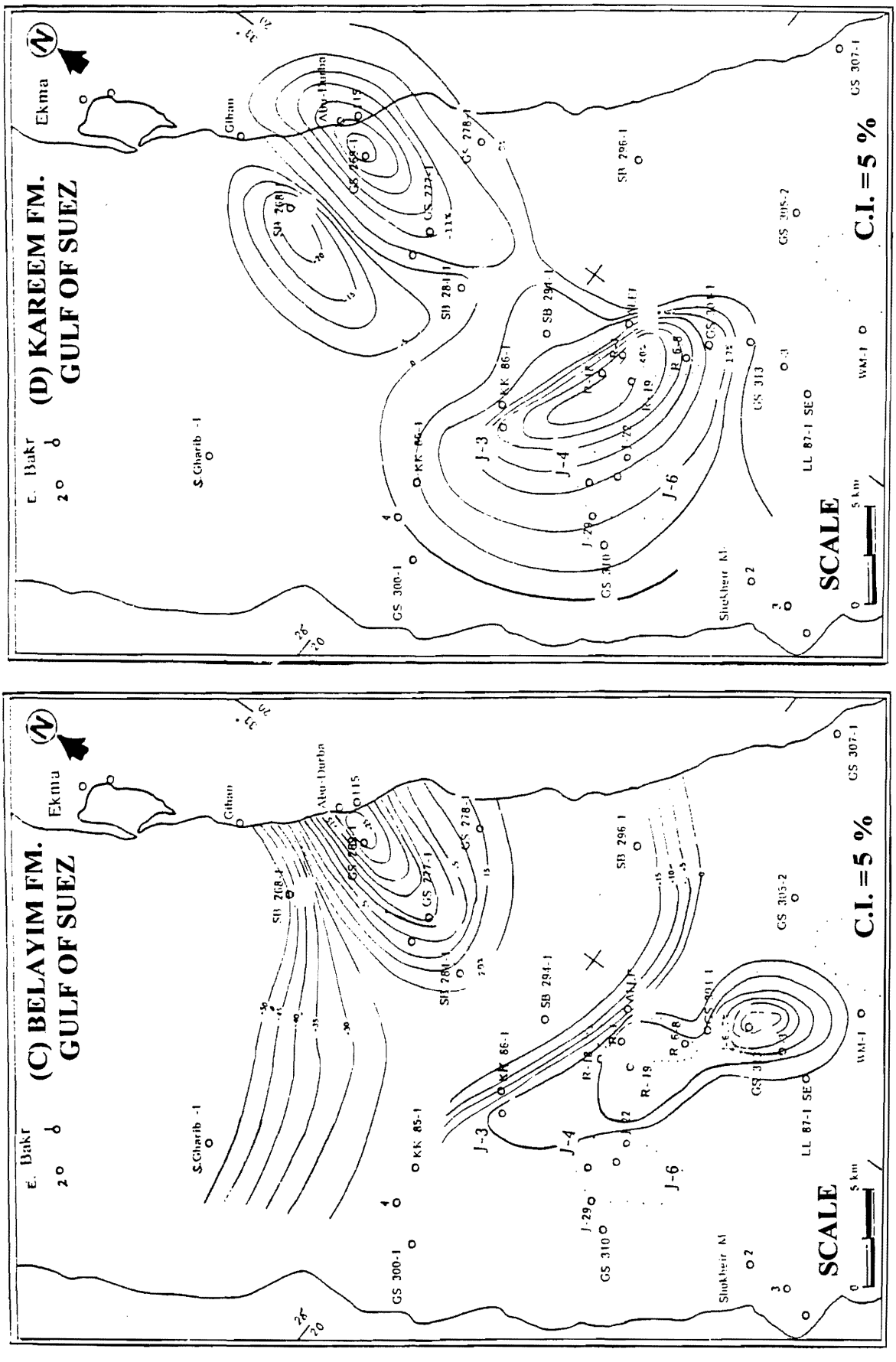

Figure 11. Discordance Map for Interval Velocity of Zeit Formation (A), South Gharib Formation (B), Belayim Formation (C), Kareem Formation (D).

is near to the shore line. From the two values of K and V_0 of the studied area, the average velocity (V) could be established at any vertical depth (ΔZ). The depth error (ΔZ) map at the top of Kareem Formation (Figure 14) is shown according to this relation:

$$\Delta Z = \left(V_{ST} - V_{RMS}\right) * T_{onewaytime} \tag{8}$$

where: V_{st} is the stacked velocity, V_{RMS} is the root mean square velocity, and T is the one-way vertical travel time. Range discrepancies can be used as an indication for lithologic changes [13] and structural anomalies.

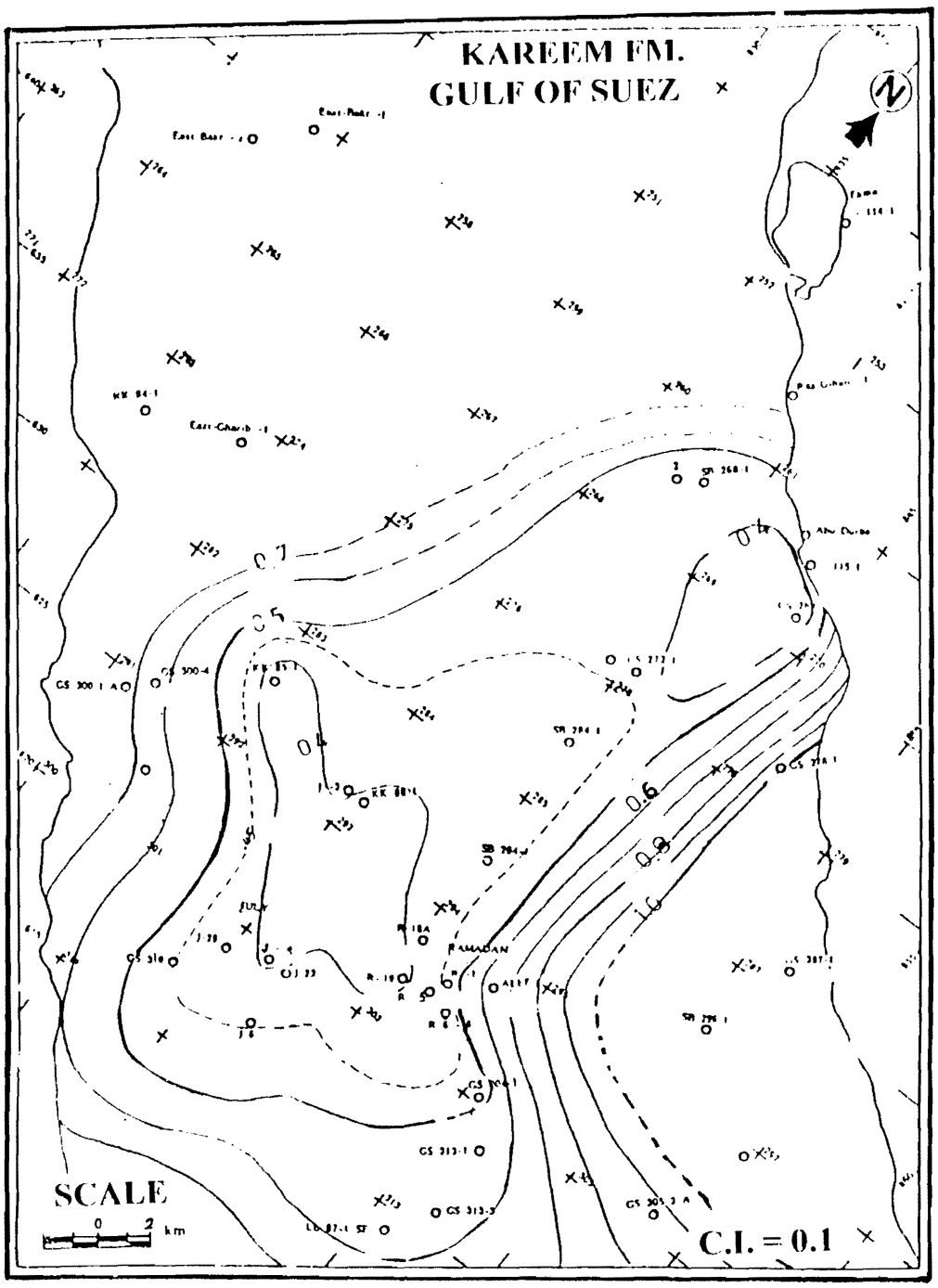

Figure 12. Velocity Gradient (K) Map of Top Kareem Formation.

ILLUSTRATIVE EXAMPLE

Modeling techniques are normally used in the seismic interpretation of the complex structures of the Gulf of Suez. A typical salt diapir structure is shown in Figure 15. Such a structure is commonly encountered in the Gulf of Suez. In such a case, the salt dome has significantly high velocity, which causes a large velocity contrast with the surrounding layers. The precise definition of the flanks of the salt domes is of economic importance, because the hydrocarbon occurrences are often found immediately adjacent to the salt dome. Stacking velocity in this case is not necessarily a single value, specially when events spread from different directions. The interpreted seismic section of line W79-88/2-1 is shown in Figure 15.

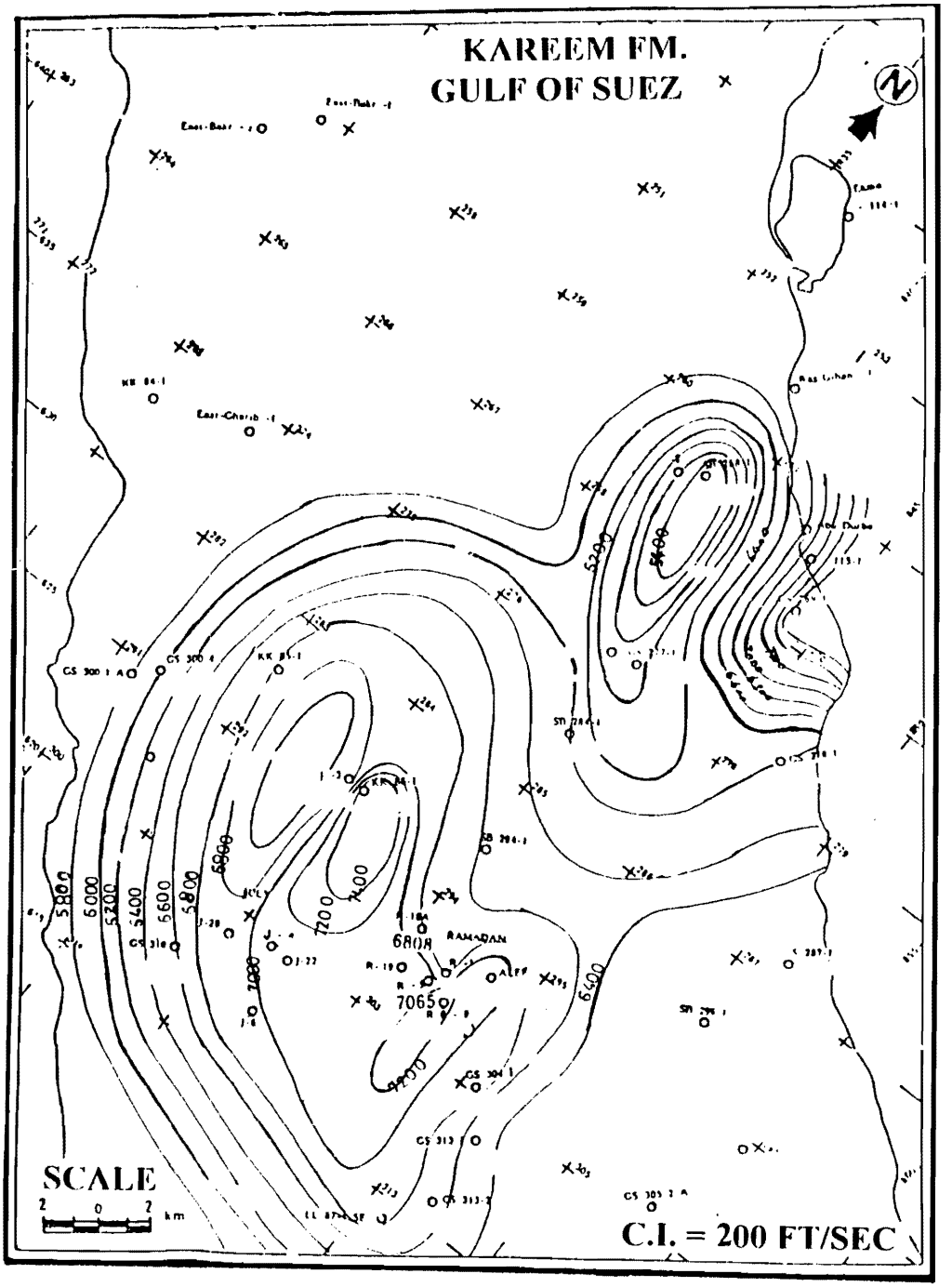

Figure 13. Velocity at Datum V_0 of Top Kareem Formation.

A preliminary stack of the seismic section W79-88/2-1 was used to check the effectiveness of the various processing steps and in diagnosing the additional problems. So, the selected velocity panel is important to observe the lateral velocity variations along the seismic profile. Velocity analysis at selected points was performed and a display of the variable stacking velocities made (Figure 16), by using the interpolated CDP's [16].

Seismic data in the Gulf of Suez are affected by two severe problems which hinder the interpretation of the complex geology. First, the shallow Middle Miocene (Zeit Formation) and Recent alternating clastic and non-clastic deposits form a strong short-period multiple generator and high-cut frequency filter [17]. Second, the underlying Middle Miocene (South Gharib Formation) in the central part of the Gulf of Suez is commonly formed into the diapiric salt structures in various

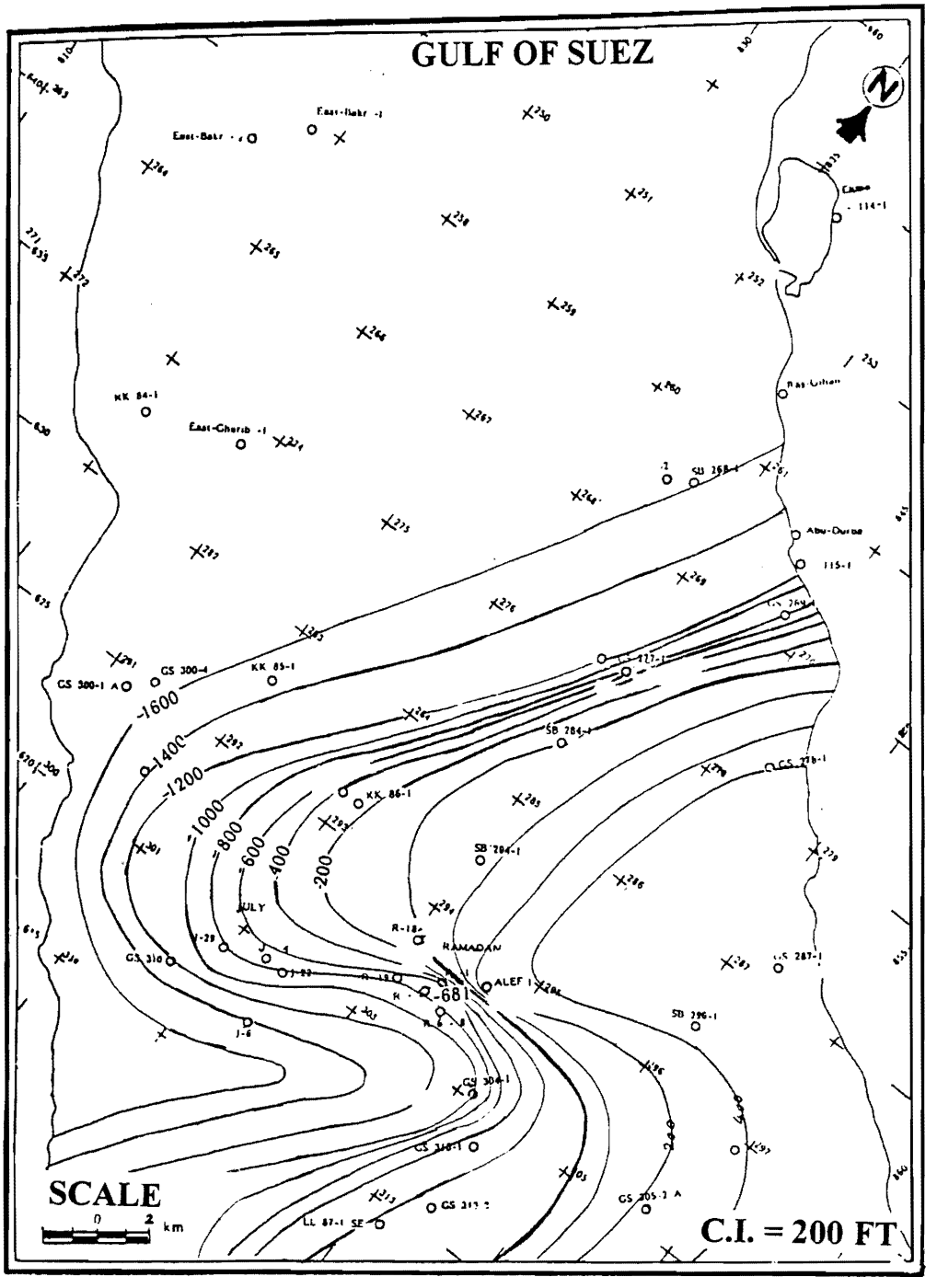

Figure 14. Depth Error (ΔZ) Map of Top Kareem Formation.

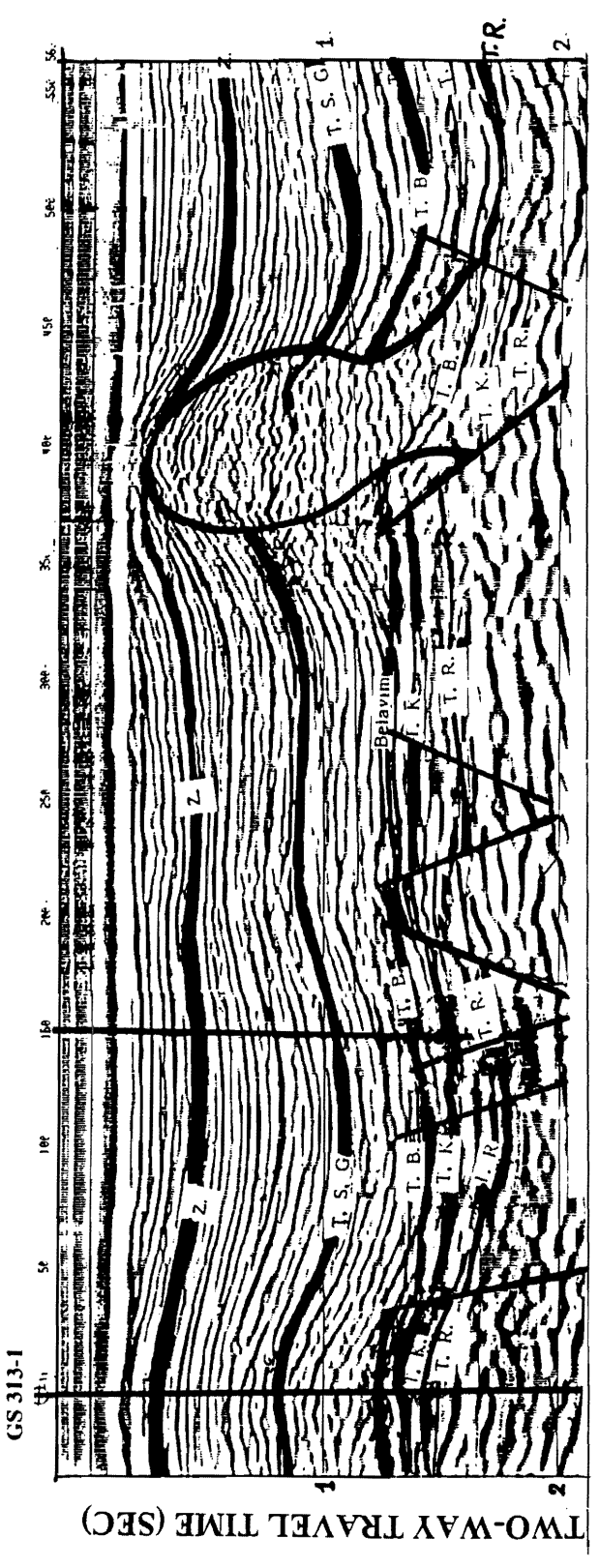

Figure 15. Interpreted Seismic Section, Line W79-88/2-1.

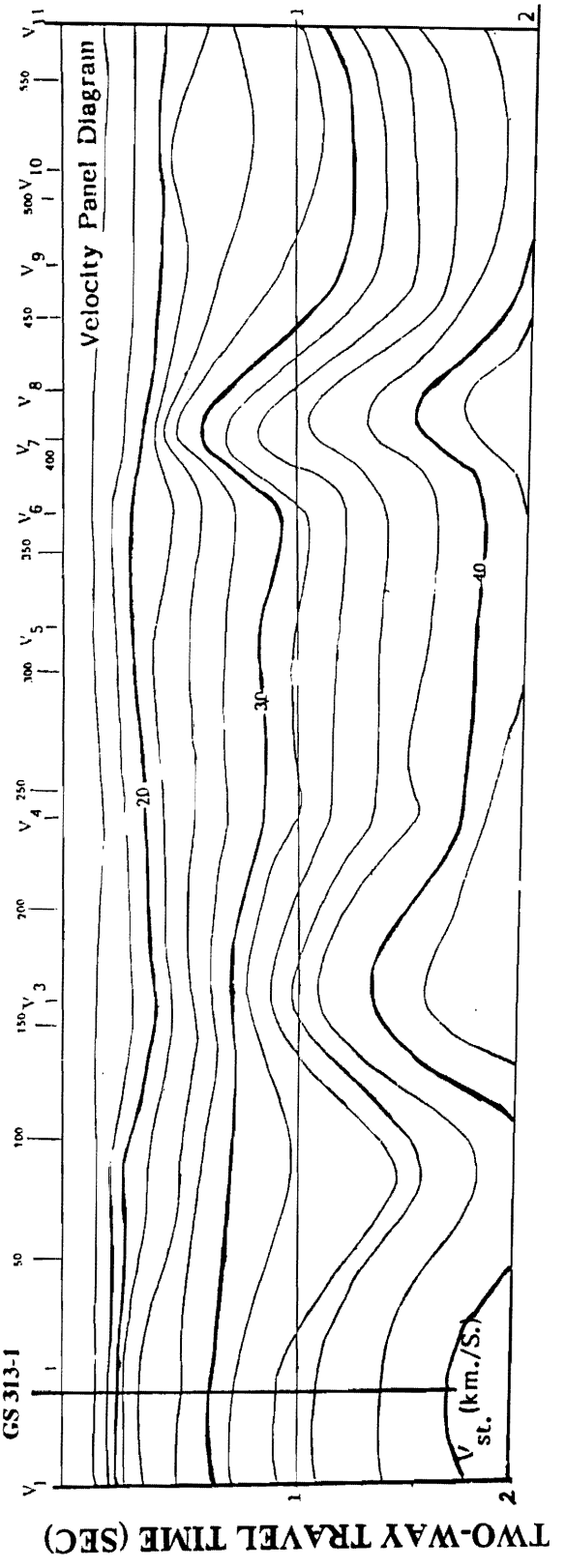

Figure 16. Variable Stacking Velocity, Line W79-88/2-1.

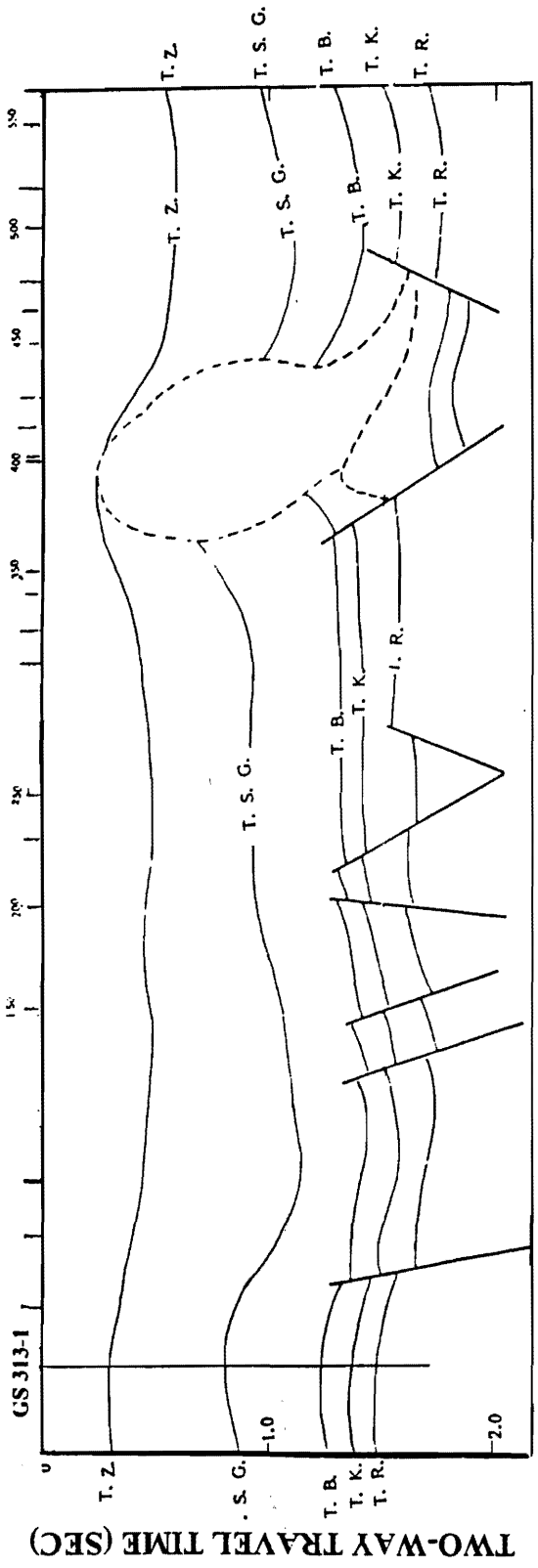

Figure 17. Interpreted Geo-Seismic Section, Line W79-88/2-1.

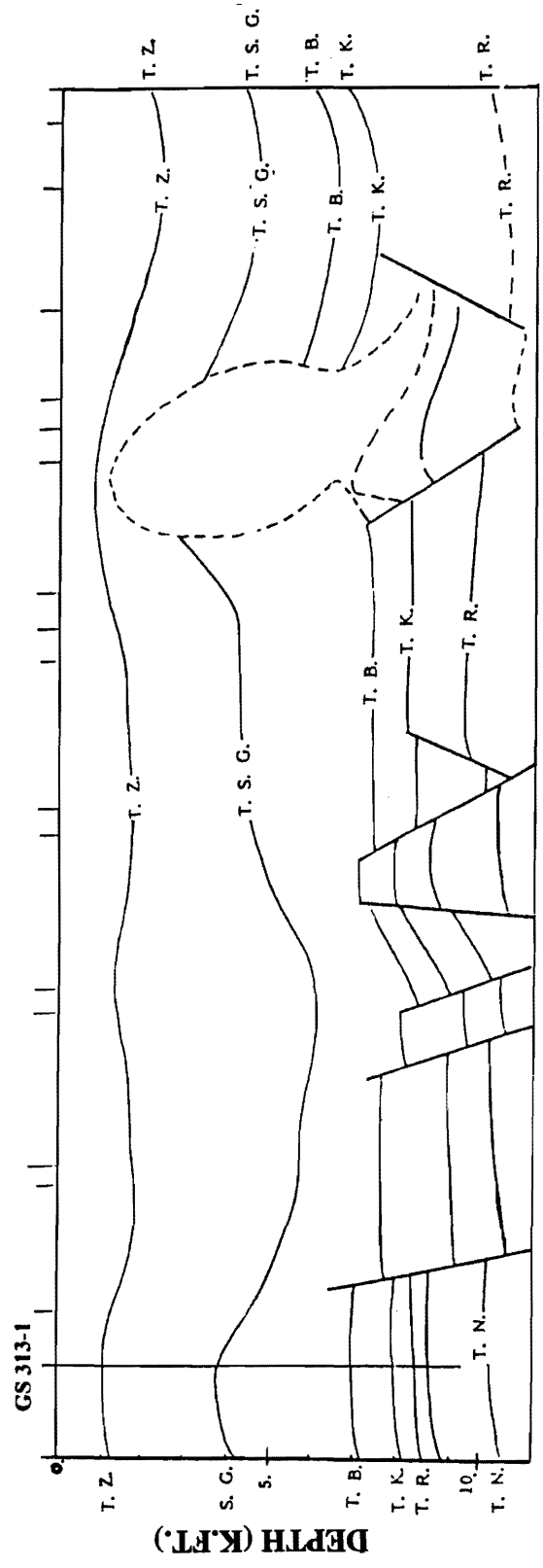

Figure 18. Depth Conversion of Seismic Section, Line W79-88/2-1.

degrees of development. Where the diapirs have developed into steep-sided features, large lateral velocity inhomogenities occur and the seismic raypaths become complex. This causes a break-down in the assumptions used in the CMP stacking process and in time-migration algorithms.

The seismic section W79-88/2-1 was processed by a wave-equation migration to eliminate the diffractions from the salt intrusion. The stack-time variant filter (STVF) was applied to suppress the noises all over the section. During the interpretation, the salt intrusion in the right part of the section was clearly recognized.

Simple time-to-depth conversion of the pre-salt reflectors yielded dips far too steep when compared to nearby wells on the same structural trend [18]. Figure 17 shows the interpreted seismic time section. A series of steep faults are terminated by the salt dome. The depth conversion of the seismic section of line W79-88/2-1 (Figure 18) was constructed from the interpreted seismic section (Figure 15) with the variable stacking velocity (Figure 16).

CONCLUSIONS

The acoustic impedance increases from the Post-Zeit section down to South Gharib rock units, but in Belayim Formation the positive values are observed only at the central part and the negative values are found elsewhere. From the seismic point of view, the reflectors from the Post-Zeit down to the base of South Gharib Formation are relatively strong and from the top of Belayim Formation downwardly the reflectors become weak for the absence of high velocity and density contrasts in the clastic sediments.

The transmission coefficient maps on the tops of Zeit and South Gharib Formations reach the maximum loss of energy due to the cyclic nature of the thin layers, exhibiting transitional interfaces of salt and shale. But in Belayim and Kareem Formations, the rate of energy loss is small. The rate of seismic energy loss in the central part is considerable and decreases toward the shore line. So the processing steps should be completely different in the two parts. In the central part of the gulf, the high velocity gradient (due to massive rocks) decreases in all directions (due to loose sediments).

Between the drilled wells the root mean square velocity is applied, because the measured average velocities are not normally available. The discordance maps of velocities show that most deviations are negative *i.e.* the surface seismic velocity survey generally yields longer velocities than the well velocity survey. In other words, the stacking velocities are in error and must be corrected by taking into account the well velocity surveys.

The relation between velocity and depth is linear for the wells: $V_{av} = V_0 + KZ$. Constructing the depth error map to the top of Kareem Formation is very useful to find the actual depth, when using the RMS velocities for converting the time to depth.

Finally, the studied area was classified into six basins trending in the NW-direction. The depth conversion of the seismic section of line W79-88/2-1 is constructed by using the interpreted seismic section with variable stacking velocity. Miocene salts cause not only structural deformation in the post-salt sections but also severe time distortions of the pre-salt reflections. Velocity discrimination is required for imaging complex structures beneath severe lateral velocity inhomogeneities. Comparison of the events on the stacked and migrated sections through the salt diapir has made it obvious that the time migration was inadequate and a depth migration process was required.

ACKNOWLEDGEMENT

I would like to express my deepest gratitude to Prof. Abu El-Ata A.S.A. for his guidance, discussion, and review of this paper.

REFERENCES

[1] M.G. Barakat, "General Review of the Petroliferous Provinces of Egypt with Special Emphasis on Their Geological Setting and Oil Potentialities. Research Project on Resource Development and Policy in Egypt", *Petroleum and Natural Gas, Cairo, Egypt,* June 1982, pp. 1–78.

[2] Schlumberger, *Well Evaluation Conference, Egypt.* Schlumberger Middle East, 1984.

[3] M.A. Ismail, "Refined Structural Imaging of South Belayim Area, Gulf of Suez, Based on Seismic Data", *Proc. E.G.S. 13th Ann. Meet,* 1995*a*, pp. 155–174.

[4] R. Said, *The Geology of Egypt.* Amsterdam, New York: Elsevier Publ. Co., 1962.

[5] B. Gutenberg, "The Amplitude of Waves to be Expected in Seismic Prospecting", *Geophysics,* **1** (1936), pp. 252–256.

[6] R.E. Sheriff, *Encyclopedic Dictionary of Exploration Geophysics, Third Edn.* Tulsa, USA: SEG, 1991.

[7] R.F. O'Doherty and N. A. Anstey, "Reflections on Amplitudes", *Geophys. Prosp.*, **19** (1977), pp. 430–458.

[8] P. Hubral and T. Krey, *Interval Velocities from Seismic Reflection Time Measurements.* Soc. Exploration Geophysicists, 1980.

[9] J.R. Coffeen, *Seismic Exploration Fundamentals.* Tulsa, Oklahoma: Pennwell Books, 1978.

[10] C.H. Dix, "Seismic Velocities from Surface Measurements", Geophysics, **20** (1955), pp. 68–86.

[11] N.A. Anstey, *The New Seismic Interpreter.* Boston, Mass: Human Resources Development Corporation, 1977.

[12] K.J. Dodds, *Seismic Applications and Interpretation.* Schlumberger Publications, 1982.

[13] N. C. Banik, "Velocity Anisotropy of Shales and Depth Estimation in the North Sea Basin", *Geophysics,* **49(9)** (1984), pp. 1411–1419.

[14] A.S.A. Abu El-Ata, A.E. Ghoneimi, and S.S. Azzam, "The Impact of Lithologic Heterogeneity on the Seismic Velocity Optimization of the Nile Delta Section of Egypt", (1995), (in press).

[15] Herrenhefer and Ostrander, *Effect of Elliptical Velocity Anisotropy on Surface Velocity Measurements.* SEG, 1973.

[16] M.A. Ismail, "Trace Interpolation Intelligent to Solve Some Seismic Interpretation Problems", *Proc. E.G.S. 13th Ann. Meet,* 1995*b*, pp. 193–204.

[17] R. Marschall and B. Fience, "An Innovative Approach to Seismic Data Acquisition and Processing in the Gulf of Suez", *Presented at the 7th Exploration Conference, EGPC, Cairo, Egypt,* 1984.

[18] P.G. Western and G. Ball, "3D Pre-stack Depth Migration in the Gulf of Suez. A Case History", *54th Meeting and Technical Exhibition, E. A. E. G.,* Paris, France, 1992.

Paper Received 18 February 1997; Revised 18 August 1997; Accepted 13 December 1997.